

1 **Intermediate water masses, a major supplier of oxygen for the eastern tropical Pacific ocean**

2 Olaf Duteil (oduteil@geomar.de)(1), Ivy Frenger(1), Julia Getzlaff(1)

3 (1) GEOMAR, Kiel, Germany

4

5 **Abstract**

6 It is well known that Intermediate Water Masses (IWM) are sinking in high latitudes and ventilate
7 the lower thermocline (500 – 1500 m depth). We here highlight how the IWM oxygen content and
8 the IWM pathway along the Equatorial Intermediate Current System (EICS) towards the eastern
9 tropical Pacific ocean are essential for the supply of oxygen to the lower thermocline and the
10 Oxygen Minimum Zones (OMZs). To this end, we assess here a heterogeneous subset of ocean
11 models characterized by a horizontal resolution ranging from 0.1° to 2.8°. Subtropical oxygen
12 levels in the lower thermocline, i.e., IWM are statistically correlated with tropical oxygen levels and
13 OMZs. Sensitivity simulations suggest that the oxygen biases of the subtropical IWM oxygen levels
14 contribute to oxygen biases of the tropical thermocline : an increase of the IWM oxygen by 60
15 mmol.m⁻³ results in a 10 mmol.m⁻³ increase in the tropical ocean in a timescale of 50 years. In the
16 equatorial regions, the IWM recirculates into the Equatorial Intermediate Current System (EICS).
17 By comparing tracer and particle release simulations, we show that a developed EICS increases
18 eastern tropical ventilation by 30 %. Typical climate models lack in representing crucial aspects of
19 this supply: biases in IWM properties are prominent across climate models and the EICS is
20 basically absent in models with typical resolutions of ~1°. We emphasize that these biases need to
21 be reduced in global climate models to allow reliable projections of OMZs in a changing climate.

22

23 **1. Introduction**

24 Oxygen levels in the ocean are characterized by high values in the high latitudes and the subtropical
25 gyres, while concentrations decrease to close to zero in the tropical oceans in the Oxygen Minimum
26 Zones (OMZs). While OMZs are natural features, climate change is potentially responsible for their
27 expansion (Breitburg et al., 2018), leading to a reshaping of the ecosystems and a potential loss of
28 biodiversity. In order to perform robust projections there is a need to better understand the processes
29 at play that are responsible for the supply of oxygen to the OMZ. We focus here on the Pacific
30 ocean, where the largest OMZs are located (Karstensen et al., 2008; Paulmier and Ruiz-Pino. 2009)

31

32 Oxygen rich waters are supplied into the ocean by subduction processes (Karstensen et al., 2008).
33 Oxygen solubility increases with lower temperatures, thus waters formed in the Southern Ocean and
34 in the North Pacific are characterized by particularly high oxygen values. In particular, the Antarctic

35 Intermediate Water (AAIW) (Molinelli, 1981) ventilates large areas of the lower thermocline of the
36 Pacific Ocean (Sloyan and Rintoul., 2001) and is characterized by oxygen values larger than 300
37 mmol.m^{-3} at subduction time (Russel and Dickson, 2003). The oxygenated core of the AAIW in the
38 tropical Pacific is located at about 500-1200 m depth at 40°S (Russell and Dickson, 2003) and with
39 this at a depth directly below the depth of the OMZs in the eastern Pacific; the Pacific AAIW mixes
40 down to 2000 m depth with the Pacific Deep Water (PDW) as determined by the OMP (Optimum
41 Multiparameter) analysis (Pardo et al., 2012; Carrasco et al., 2017). The oxygen rich (> 200
42 mmol.m^{-3} at 40°S) AAIW spreads from its formation side in the Southern Ocean to the subtropical
43 regions ; conversely the oxygen poor PDW (below 150 mmol.m^{-3}), extends till 3000m depth and
44 recirculates poleward (Koshlyakov and Tarakanov, 2003). The northern part of the Pacific basin is
45 characterized by the North Pacific Intermediate Water (NPIW) (Talley, 1993) confined to the
46 northern Pacific conversely to the AAIW, which spreads far northward as its signature reaches 15°N
47 (Qu and Lindstrom., 2004). AAIW, NPIW and the upper part of the PDW are oxygenated water
48 masses occupying the lower thermocline between 500 and 1500 m depth. We will refer to these
49 waters as Intermediate Water Masses (IWM) in the following.

50

51 In the subtropics, the IWM (more particularly the AAIW) circulates into the intermediate flow of
52 the South Equatorial Current and the New Guinea Coastal Undercurrent (Qu and Lindstrom, 2004)
53 where it retroflects in the zonal equatorial flows of the Southern Intermediate Countercurrent
54 (SICC) and Northern Equatorial Intermediate Current (NEIC) within about $\pm 2^\circ$ off the equator
55 (Zenk et al., 2005; Kawabe et al., 2010) (Fig 1). These currents are part of the Equatorial
56 Intermediate Current System (EICS) constituted by a complex system of narrow jets extending
57 below 500 m in the lower thermocline (Firing, 1987; Ascani et al., 2010; Marin et al. 2010; Cravatte
58 et al., 2012, 2017; Menesguen et al., 2019). While the existence of this complex jet system has been
59 shown to exist in particular using argo floats displacements (Cravatte et al., 2017) the spatial
60 structure and variability of the jets are still largely unknown. In addition, there is little knowledge
61 about their role in transporting properties such as oxygen.

62

63 The simulation of the supply of oxygen to the eastern tropical Pacific is a difficult task as it depends
64 on the realistic simulation of the IWM properties (in particular the oxygen content) and the IWM
65 pathway (through the EICS). It is known that current climate models, in particular CMIP5 (Coupled
66 Model Intercomparison Project phase 5) models, have deficiencies in correctly representing the
67 IWM, and in particular the AAIW. They generally display too shallow and thin IWM, with a
68 limited equatorward extension compared to observations (Sloyan and Kamenkovich, 2007; Sallee et

69 al., 2013; Meijers, 2014; Cabre et al., 2015; Zhu et al., 2018 for the south Atlantic ocean).
70 Discrepancies in the simulated properties of IWM compared to observations are due to a
71 combination of many errors in the climate models, including simulation of wind and buoyancy
72 forcing, inadequate representation of subgrid-scale mixing processes in the Southern Ocean, and
73 midlatitude diapycnal mixing parameterizations (Sloyan and Kamakovich, 2007; Zhu et al., 2018).
74 In addition, the representation of the EICS is lacking in coarse resolution models (Dietze and
75 Loeptien, 2013; Getzlaff and Dietze, 2013). Higher resolution (0.25°, 1/12°) configurations partly
76 resolve the EICS but with a smaller amplitude than observed (Eden and Dengler, 2008; Ascani et
77 al., 2015). The mechanisms forcing the EICS are complex and still under debate (see the review by
78 Menesguen et al., 2019).

79

80 In this study we focus on the impact of IWM (and of the deficiencies in the representation of their
81 properties and transport) on the oxygen content in the eastern tropical Pacific in a set of model
82 simulations. Section 2 gives an overview of all models that we used as well as of the sensitivity
83 simulations. Next, we assess to which extent the IWM modulate (or drive) the oxygen levels in the
84 eastern tropical (20°S – 20°N; 160°W-coast) Pacific ocean in this set of models. The role of the
85 IWM depends i) on the oxygen content of the IWM in the lower thermocline of the subtropical
86 regions (section 3) and ii) on the zonal recirculation of the oxygen by the EICS toward the
87 easternpart of the basin (section 4). We conclude in section 5.

88

89 **2. Analyzed models and experiments**

90 2.1 Mean state

91 We analyze the mean state of the oxygen fields, OMZ, EICS of the following model experiments
92 (see Table 1), which previously have been used in recent studies focusing on the understanding of
93 the tropical oxygen levels mean state or variability :

94 - the NEMO (Nucleus for European Modelling of the Ocean) model (Madec et al., 2017) with a
95 resolution of 2°, refined meridionally to 0.5° in the equatorial region (NEMO2 configuration). The
96 circulation model is coupled to a simple NPZD (Nutrient Phytoplankton Zooplankton Detritus)
97 biogeochemical model that comprises 6 compartments (e.g used in Duteil et al., 2018; Duteil,
98 2019). The simulation has been forced by climatological forcings based on the Coordinated
99 Reference Experiments (CORE) v2 reanalysis (1948-2007) (Large and Yeager, 2009) and
100 integrated for 1000 years.

101 - the UVIC (University of Victoria) model (e.g used in Getzlaff et al., 2016; Oschlies et al., 2017),
102 an earth System Model (ESM) that has a horizontal resolution of 1.8° latitude x 3.6° longitude. The

103 experiment has been integrated for 10000 years. The biogeochemical model is a NPZD-type model
104 of intermediate complexity that describes the full carbon cycle (see Keller et al., 2012 for a detailed
105 description). This model is forced by monthly climatological NCAR/NCEP wind stress fields.

106 - the GFDL (Geophysical Fluid Dynamics Laboratory) CM2-0 suite (Delworth et al., 2012; Griffies
107 et al., 2015, Dufour et al, 2015): the suite is based on the GFDL global climate model and includes
108 a fully coupled atmosphere with a resolution of approximately 50 km. It consists of three
109 configurations that differ in their ocean horizontal resolutions: GFDL1 with a nominal 1°
110 resolution, GFDL025 with a nominal 0.25° and GFDL01 with a nominal 0.1° resolution (e.g used in
111 Frenger et al., 2018 and Busecke et al., 2019 for studies on ocean oxygen). At simulation year 48,
112 the simplified ocean biogeochemistry model miniBLING is coupled to the models, with three
113 prognostic tracers, phosphate, dissolved inorganic carbon and oxygen (Galbraith et al., 2015). Due
114 to the high resolution of GFDL01, the integration time is limited. We here analyze simulation years
115 186 to 190.

116 All the models (NEMO2, UVIC, GFDL suite) are forced using preindustrial atmospheric pCO₂
117 concentrations.

118 Differences in model resolution but also in atmosphere forcings or spinup duration strongly impact
119 oxygen distribution (see Appendix A). The heterogeneity of the configurations that we analyze
120 permits to determine whether the simulated oxygen distributions display recurrent biases or
121 conversely similar patterns. The mean states of the oxygen distributions are discussed below in
122 section 3.1 “IWM Oxygen levels in models”.

123

124 2.2 Sensitivity simulations

125 In order to disentangle the different processes at play we perform two different sets of sensitivity
126 simulations using the eNEMO model engine. NEMO allows to test effects of increasing the ocean
127 resolution and to integrate the model over a relatively long time span. All sensitivity experiments
128 are integrated for 60 years (1948 to 2007) using the CORE (Coordinated Ocean-Ice Reference
129 Experiments) v2 interannual (Large and Yeager, 2009) forcings. This time scale permits the
130 recirculation from the interior subtropical regions to the tropical area (as suggested in the model
131 study by SenGupta and England, 2007).

132

133 2.2.1 Oxygen forcing to observations in the subtropical regions

134 In the first set of experiments the focus is on the role of the lower thermocline oxygen content for
135 the ventilation of the eastern equatorial Pacific. We use NEMO2, the oceanic component of the

136 IPSL-CM5A (Mignot et al., 2013), that is part of CMIP5. NEMO2 shows mid-latitudes oxygen
137 biases consistent with CMIP5 models. We compare three experiments :

138 - NEMO2-REF: the experiment is integrated from 1948 to 2007 starting from the spinup state
139 described in 2.1.

140 - NEMO2-30S30N: the oxygen boundaries are forced to observed oxygen concentrations (WOA)
141 at the boundaries 30°N and 30°S: the mid-latitude supply of oxygen by the IWM is therefore
142 correctly represented.

143 - NEMO2-30S30N1500M: similar to NEMO2-30S30N. In addition oxygen is forced at the depth
144 interface of 1500m, mimicking a correct oxygen state of the deeper water masses (lower part of the
145 AAIW, upper part of the PDW)

146

147 We focus with the above three experiments on the transport of IWM oxygen levels to the tropical
148 ocean and the OMZs. The respiration rate (oxygen consumption) is identical in NEMO2-REF,
149 NEMO2-30S30N and NEMO2-30S30N1500M in order to avoid compensating effects between
150 supply and respiration that depend on biogeochemical parameterizations (e.g Duteil et al., 2012).

151 We aim to avoid such compensating effects to ease interpretation and be able to focus on the role of
152 physical transport. The sensitivity of tropical IWM oxygen to subtropical and deep oxygen levels is
153 discussed in section 3.2

154

155 2.2.2 Conservative Tracer Release in oxygenated waters

156 In a second set of experiments, we performed tracer release experiments in a coarse 0.5°
157 (NEMO05) and high resolution 0.1° (NEMO01) configuration of the NEMO model engine (Table
158 1) to examine the transport of oxygenated IWM from the subtropical regions into the oxygen
159 deficient tropics. NEMO01 is a configuration based on NEMO05 and where a 0.1° two-ways nest
160 has been embedded in the whole Pacific Ocean, from 49°S to 31°N (Czeschel et al, 2011). In these
161 experiments, we initialized the regions with climatological (WOA) oxygen levels greater than 150
162 mmol.m⁻³ with a value of 1 (and 0 when oxygen is lower than 150 mmol.m⁻³). In the model
163 simulations, the tracer is subject to the same physical processes as other physical and
164 biogeochemical tracers, i.e. advection and diffusion but it does not have any sources and sinks. The
165 experiments have been integrated for 60 years (1948 – 2007) using realistic atmosphere forcing
166 (COREv2). NEMO05 and NEMO01 display a similar upper ocean circulation (Fig 5) but NEMO05
167 does not simulate a developed EICS contrary to NEMO01.

168

169 In order to complement the tracer experiment we performed Lagrangian particle releases.
170 Lagrangian particles allow to trace the pathways of water parcels due to the resolved currents, and
171 to track the origin and fate of water parcels. They are not affected by subgrid scale mixing
172 processes. The particles are advected offline with 5days mean of the NEMO05 and NEMO01
173 currents. The NEMO01 circulation fields have been interpolated on the NEMO05 grid in order to
174 allow a comparison of the large scale advective patterns between NEMO01 and NEMO05. We used
175 the ARIANE tool (Blanke and Raynaud, 1997). A first particle release has been performed in the
176 eastern tropical OMZ at 100°W in the tropical region between 5°S - 5°N, a second release has been
177 performed in the western part of the basin at 160°E. The particles have been released in the lower
178 thermocline at 1000 m and integrated backward in time from 2007 to 1948 in order to determine
179 their pathways and their location of origin. We released 120 particles every 5 days during the last
180 year of the experiment, for a total of 8760 particles. The transport by the EICS is discussed in
181 section 4.2 (“tracers levels and Lagrangian pathways”).

182

183 **3. Intermediate water properties and oxygen content**

184 3.1. IWM Oxygen levels in models

185 The IWM subducted in mid/high latitudes are highly oxygenated waters. As part of the deficient
186 representation of IWM, the subducted “oxygen tongue” (oxygen values up to 240 mmol.m⁻³) is not
187 reproduced in most of the models part of CMIP5 (Fig 8 from Cabre et al., 2015, Fig 4 from Takano
188 et al., 2018) and in the models analyzed here (Fig 2a), with biases of about 20-60 mmol.m⁻³
189 (NEMO2, GFDL1, GFDL025, GFDL01). UVIC, a coarse resolution model, shows oxygenated
190 waters in the lower thermocline at mid latitudes (30°S-50°S); the oxygenation however arises due to
191 a too large vertical diffusion from the mixed layer rather than by an accurate representation of the
192 water masses.

193

194 GFDL01, even though still biased low, presents larger oxygen values than the coarser resolution
195 models GFDL1, GFDL025 and NEMO2. A possible explanation is a better representation of the
196 water masses and in particular the AAIW in eddy-resolving models (Lackhar et al., 2009).

197

198 The IWM oxygen maximum is apparent at 30°S throughout the lower thermocline (600 – 1000 m)
199 in observations (Fig 2b), consistent with the circulation of IWM with the gyre from the mid/high
200 latitude formation regions towards the northwest in subtropical latitudes, and followed by a
201 deflection of the waters in the tropics towards the eastern basin. This oxygen peak is missing in all
202 the models analyzed here.

203

204 Consistent with the low oxygen bias of models at subtropical latitudes (Fig 2b), models also feature
205 a bias in the tropical ocean (20°S-20°N) by 20 – 50 mmol.m⁻³ (Fig 2a, Fig 2c) at intermediate depths
206 in the eastern part of the basin (similarly to CMIP5 models, as shown by Cabre et al., 2015). The
207 basin zonal average of the mean oxygen level in the lower thermocline (layer 500 - 1500) m at 30°S
208 and in the eastern part of the basin (average 20°S – 20°N, 160°W-coast; 500-1500 m) are positively
209 correlated (Pearson correlation coefficient R=0.73) (Fig 2d, Appendix A), suggesting a large role of
210 the IWM in controlling the oxygen levels in the tropical oceans.

211

212 The models presenting the poorest oxygenated water at 30°S display the largest volume of OMZs
213 (GFDL025 and GFDL1), though the negative correlation (Pearson correlation coefficient R=-0.52)
214 is less pronounced between the volume of the OMZs and the mean oxygen levels in the layer 500 -
215 1500 m at 30°S (Fig 2e). Reasons of this weaker correlation are due to the OMZs being a result of
216 several processes next to oxygen supply by IWM, e.g, vertical mixing with other water masses
217 (Duteil et al., 2011), isopycnal mixing in the upper thermocline (Gnanadesikan et al., 2013; Bahl et
218 al., 2019), supply by the upper thermocline circulation (Shigemitsu et al., 2017; Busecke et al.,
219 2019). A correlation, even weak, suggests a major role of the IWM in regulating the OMZ volume.

220

221 In order to better understand the role of IWM entering the subtropical domain from higher latitudes
222 for the oxygen levels in the eastern tropical Pacific Ocean, we perform sensitivity experiments (see
223 2.2.1) in the following.

224

225 3.2 Sensitivity of tropical IWM oxygen to subtropical and deep oxygen levels

226 3.2.1 Oxygen levels in the lower thermocline

227 The difference of the experiments NEMO2-30S30N – NEMO2-REF (average 1997-2007) (Fig
228 3c,d) allows to quantify the effect of model biases of IWM at mid latitudes (30°N/30°S). As we
229 restore oxygen to observed levels at 30°S/°N (see 2.2.1), the difference shows a large anomaly in
230 oxygen levels at 30°S (more than 50 mmol.m⁻³) at lower thermocline level (500 – 1500 m)
231 corresponding to the missing deep oxygen maximum . The northern negative anomaly results from
232 a deficient representation of the north Pacific OMZ, i.e., modeled oxygen is too high for NPIW. The
233 northern low and southern high anomalies spread towards the tropics at intermediate depth. A
234 fraction of the positive oxygen anomaly recirculates at upper thermocline level due to a
235 combination of upwelling and zonal advection by the tropical current system (for instance the EUC

236 at thermocline level is a major supplier of oxygen as shown in observations by Stramma et al., 2010
237 and in ocean models by Duteil et al., 2014, Busecke et al., 2019).

238

239 The difference NEMO2-30S30N1500M – NEMO2-30S30N (Fig 3e,f) shows a deep positive
240 anomaly in oxygen, as oxygen levels are lower than in observations by 30-40 mmol.m⁻³ in the
241 eastern tropical regions. This anomaly is partially transported into the lower thermocline (500 -
242 1500 m). It shows that a proper representation of the deep oxygen level (> 1500 m) is important for
243 a realistic representation of the lower thermocline and OMZs. Causes of the oxygen bias of the
244 deeper water masses are beyond the scope of this study but may be associated with regional
245 (tropical) issues, such as an improper parameterization of respiration (e.g a too deep
246 remineralisation) (Kriest et al., 2010), or a misrepresentation of deeper water masses.

247

248 3.2.2 Oxygen budget and processes

249 To assess the processes that drive the oxygen content of the (sub)tropical lower thermocline, we
250 analyzed the oxygen budget in NEMO2-REF and NEMO2-30S30N. The budget is computed as an
251 average between 500 and 1500m and shown in Fig 3g and Fig.4.

252

253 The oxygen budget is :

$$254 \frac{\delta O_2}{\delta t} = Adv_x + Adv_y + Adv_z + Diff_{Dia} + Diff_{Iso} + SMS$$

255 where Adv_x, Adv_y, Adv_z , are respectively the zonal, meridional and vertical advection terms, $Diff_{dia}$
256 and $Diff_{iso}$ are the diapycnal and isopycnal diffusion terms. SMS (Source Minus Sink) is the
257 biogeochemical component (i.e respiration below the euphotic zone)

258

259 In NEMO2-REF, the physical oxygen supply is balanced by the respiration. The oxygen supply in
260 the model is divided into advection, i.e., oxygen transport associated with volume transport, and
261 isopycnal diffusion, i.e., subgrid scale mixing processes that homogenize oxygen gradients (Fig 4a).
262 Diapycnal diffusion is comparatively small and can be neglected. The lower branches of the
263 subtropical gyres transport the oxygen from the eastern to the western part of the basin.
264 Downwellings from the oxygen-rich mixed layer supply the interior of the subtropical gyres. At the
265 equator, the EICS transport westward oxygen-poor water originating in the eastern side of the basin
266 (Fig 4a). Concomitantly, the meridional advection term transports oxygen originating from the
267 subtropics in the tropical regions, which is upwelled. Isopycnal diffusion transfers oxygen from the
268 oxygen-rich gyres to the poor oxygenated regions.

269

270 The anomalies generated at 30°S and 30°N by the restoring experiment generate a disbalance
271 between respiration (which remains identical in NEMO2-REF and NEMO2-30S30N) and supply.
272 This disbalance is most apparent in the tropics by an increase (south) or decrease (north) of
273 isopycnal diffusion (Fig 3g, Fig 4b). Changes in the advective terms can be found along the equator:
274 as the vertical gradient of oxygen decrease (the intermediate ocean being more oxygenated), the
275 vertical supply from the upper ocean decreases in the south (increases in the north) subtropical gyre
276 and decreases at the equator (Fig 4b). The meridional oxygen gradient between the southern
277 subtropical gyre and the equator strengthens, and so the meridional transport from the subtropics to
278 the equator, partly by the western boundary currents. The changes in zonal transport are
279 comparatively small. The total advective term does not present significant change however.

280

281 In the experiment NEMO2-30S30N1500, in complement to the isopycnal propagation of the
282 subtropical anomaly, the deep (> 1500 m) oxygen anomaly is upwelled in the eastern equatorial
283 (500 – 1500 m) part of the basin (see Fig 3g) showing a large increase in advective terms, mostly
284 due to an increase in vertical advection), consistent with the analysis by Duteil (2019) who showed
285 that vertical advection is the dominant process to supply oxygen from the lower to the upper
286 thermocline in the equatorial eastern Pacific Ocean in a similar NEMO2 configuration.

287

288 This simple set of experiment shows that in climate models oxygen in the lower thermocline (500 –
289 1500 m) ocean are partially controlled by properties of IWM that enter the tropics from higher
290 latitudes. This presumably applies to other (biogeochemical) tracers. IWM oxygen propagates
291 equatorward mostly by small scale isopycnal processes and the western boundary currents. Further,
292 upwelling in the tropics from deeper ocean layers (Pacific Deep Water, partially mixed with the
293 lower IWM) play an important role. Our budget analysis highlighted the importance of advective
294 processes in the equatorial region in the lower thermocline which we will examine more closely in
295 the following.

296

297 **4. Equatorial intermediate current system and oxygen transport**

298 4.1 Structure of the currents in the upper 2000 m in observations and models

299 The current structure of the models analyzed in this study (see section 2.1, Table 1) is shown in Fig.
300 5. In the mixed layer, the broad westward drifting South and North Equatorial Currents (SEC, NEC)
301 characterize the equatorial side of subtropical gyres. In the thermocline, the eastward flowing
302 equatorial undercurrent (EUC), flanked by the westward flowing south and north counter currents

303 are present in all models. This upper current structure is well reproduced (i.e the spatial structure
304 and intensity are consistent with observations) across the different models (see 2.1 “Model
305 analyzed”) compared to observations. Previous studies already discussed the upper thermocline
306 current structure in the GFDL models suite (Busecke et al., 2019), NEMO2 and NEMO05 (e.g
307 Izumo, 2005, Lübbecke et al., 2008), UVIC (Loeptien and Dietze, 2013); the upper thermocline will
308 not be further discussed in this study.

309

310 At intermediate depth, in the observations, a relatively strong (about 0.1 ms^{-1}) westward flowing
311 Equatorial Intermediate Current (EIC) is present below the EUC at about 400-600 m depth (Marin
312 et al., 2010). A complex structure of narrow and vertically alternating jets every 200 m, so-called
313 Equatorial Deep Jets (EDJ), extends below the EIC till 2000 m (Firing, 1987; Cravatte et al., 2012).
314 Laterally to the EIC, in the upper thermocline, the Low Latitude Subsurface Countercurrents
315 (LLSC) are observed. They include the North and South Subsurface Counter Currents (NSCC and
316 SSCC), located around $5^{\circ}\text{N}/5^{\circ}\text{S}$, and a series of jets between $5^{\circ}\text{N}/\text{S}$ and $15^{\circ}\text{N}/\text{S}$ (in particular the
317 Tsuchiya jets in the southern hemisphere, described by Rowe et al., 2000). Below the LLSCs, the
318 Low Latitude Intermediate Currents (LLICs) include the a series of westward and eastward zonal
319 jets (500–1500-m depth range) alternating meridionally from 3°S to 3°N ; the North and South
320 Intermediate Countercurrents (NICC and SICC) flow eastward at 1.5° – 2° on both flanks of the
321 lower EIC. The North and South Equatorial Intermediate Currents (NEIC and SEIC) flow westward
322 at about 3° (Firing, 1987). A detailed schematic view of the tropical intermediate circulation is
323 shown in a recent review by Menesguen et al. (2019) and in Fig 1.

324

325 In coarse resolution models, the intermediate current system is not developed and sluggish (even
326 missing in UVIC and GFDL1). NEMO2 and NEMO05 display a “primitive” EICS as the LLSCs
327 are not represented. High resolution models (GFDL025, GFDL01, NEMO01) display a more
328 realistic picture, even if the mean velocity is still weaker than in observations (smaller than 5 cm.s^{-1}
329 ¹), where it reaches more than 10 cm^{-1} at 1000 m (Ascani et al., 2010; Cravatte et al., 2017). An
330 interesting feature is that the jets are broader and faster in NEMO01 than in GFDL01. Possible
331 causes include a different wind forcing, mixing strength or topographic features as all these
332 processes play a role in forcing the intermediate jets (see the review by Menesguen et al., 2019).
333 The intermediate currents are less consistent vertically in NEMO01 than in GFDL01, due to their
334 large temporal variability in NEMO01. A strong seasonal and interannual variability of the EICS
335 has been observed that displays varying amplitudes and somewhat positions of the main
336 currents/jets (Firing, 1998; Gouriou et al., 2006; Cravatte et al., 2017). A clear observational picture

337 of the EICS variability is however not yet available. Outside the tropics (in particular south of
338 15°S), the interior velocity pattern is similar in coarse and high resolution models, suggesting a
339 similar equatorward current transport at intermediate depth in the subtropics, in for instance
340 NEMO05 and NEMO01.

341

342 4.2 Transport by the EICS

343 4.2.1 Tracer spreading towards the eastern tropical Pacific

344 We released a conservative tracer in the subtropical domain in well oxygenated waters (see 2.2.2) in
345 a coarse (NEMO05) and a high resolution configuration (NEMO01). The tracer does not have
346 sources or sinks and is advected and mixed as any other model tracer and allows to assess the
347 spreading of tracer (such as oxygen) from oxygenated waters into the oxygen deficient eastern
348 tropical Pacific.

349

350 The ventilation by the oxygen rich waters, and in particular the IWM, is illustrated by the tropical
351 tracer concentration after 50 years (Fig 6a) of integration (mean 2002-2007). Concentrations
352 decrease from the release location to the northern part of the basin, where the lowest values (below
353 0.1) are located in NEMO05 and NEMO01. The 0.1 isoline is however located close to the equator
354 in NEMO05 while it is found around 7°N in NEMO01. This feature is associated with a pronounced
355 tongue of high tracer concentration (> 0.2) between 5°N and 5°S in NEMO01. Such a tongue is
356 absent in NEMO05. The enhanced tracer concentration in the equatorial region suggests a stronger
357 equatorial ventilation in NEMO01.

358

359 The preferential pathways of transport are highlighted by the determination of the transit time it
360 takes for the tracer to spread from the oxygen rich regions to the tropical regions. We define a
361 threshold called $t_{10\%}$ when the tracer reaches a concentration of 0.1 (Fig 6b) (similar to the
362 approach of SenGupta and England, 2007). $t_{10\%}$ highlights a faster ventilation of the equatorial
363 regions in NEMO01 compared to NEMO05, as $t_{10\%}$ displays maximum value of 10 (western part)
364 to 30 years (eastern part) between 5°N/5°S in NEMO01 compared to 30 years to more than 50 years
365 in NEMO05. The southern “shadow zone” is well individualized in NEMO01 compared to
366 NEMO05 as the oxygen levels are high in the equator in NEMO01, suggesting a strong transport by
367 the EICS. While $t_{10\%}$ increases linearly at intermediate depth at 100°W in NEMO05 from 20°S to
368 the equator, suggesting a slow isopycnal propagation (consistent with the experiments performed
369 using NEMO2 in part 3.2), the tracer accumulation is faster in the equatorial regions than in the

370 mid-latitudes in NEMO01, suggesting a large role of advective transport, faster than a transport by
371 diffusive processes.

372

373 4.2.2 Equatorial lower thermocline water mass origin

374 Lagrangian Particles (see 2.2.2) allow us to understand the origin of the waters in the lower
375 thermocline. They also allow to disentangle the transport of the resolved currents of the EICS
376 (advection) from subgrid scale mixing processes, i.e. to assess the processes responsible for the
377 equatorial ventilation. Two releases R1 and R2 have been performed in the eastern and western part
378 of the basin in order to assess the equatorial circulation in NEMO05 and NEMO01.

379

380 The release R1 (100°W, 5°N-5°S, 1000 m depth) is included in the larger Intermediate Eastern
381 Tropical Pacific (IETP) ocean region (160°W – coast / 10°N-10°S / 200 – 2000 m).The particles
382 originate close to the region of release (IETP) in 60 % of the cases in NEMO05 and 50 % of the
383 cases in NEMO01, at a time scale of 50 years (Fig 7a and 8b). In NEMO05, after 50 years, the
384 particles originating outside the IETP come either from the upper (0 – 200 m) ocean (5 %), deep (>
385 2000 m) ocean (1%), higher (> 10°) latitudes (23 %), western (west of 160°W) part of the basin (21
386 %) (Fig 8d). The largest difference between NEMO05 and NEMO01 is the much larger amount of
387 particles originating from the deep ocean in NEMO01 (8 % in NEMO01), suggesting the presence
388 of vertical recirculation cells at intermediate depths. The advection processes are also considerably
389 faster in NEMO01, in particular the zonal advective ones. The relative difference between
390 NEMO05 and NEMO01 is particularly strong 15 years after the release (approximately
391 corresponding to the t10% at 1000 m at the equator in NEMO01), as already 10 % of the particles
392 originate outside the IETP, in regions where the oxygen levels are high, in NEMO01 while this
393 fraction is close to 0 in NEMO05.

394

395 The location of the second release R2 (160°E, 5°N-5°S, 1000 m depth) is included in the
396 Intermediate Western Tropical Pacific (IWTP) ocean region (160°W – coast / 10°N-10°S / 200 –
397 2000 m) (Fig 7b). After 50 years, all the particles originate outside of the IWTP in NEMO01 (Fig
398 8c) (50 % originate in the eastern basin, 23 % in the deep ocean, 24 % outside the equatorial band, 3
399 % in the upper 200 m) (Fig 8e) while only 70 % of the particles originate outside the IWTP in
400 NEMO05 (39 % in the eastern basin, 27 % outside the equatorial band, 2 % in the deep ocean and 2
401 % in the upper ocean).

402

403 The Lagrangian experiments point to a generally stronger ventilation at intermediate depth in
404 NEMO01 due to the EICS, which reinforces the connections between western / eastern part of the
405 basin and thermocline / deep ocean.

406

407 4.3 Equatorial oxygen levels in models

408 Our analyses above permit to better understand the distribution of the oxygen levels at the equator
409 in a suite of models characterized by an increasing resolution, such as the GFDL model suite. The
410 striking difference between GFDL01 and GFDL025 / GFDL1 are the high oxygen levels in the
411 eastern part of the ocean below 1000 m in GFDL01 compared to GFDL025/GFDL1 (Fig 2). The
412 oxygen levels are also more homogeneous zonally in GFDL01, with a weaker east/west gradient,
413 consistent with the tracer experiment that we performed in 4.2. The oxygen distribution fits with the
414 mean kinetic energy of the intermediate currents below 1000 m (Fig 9a), especially in the eastern
415 part of the basin (Fig 9b). Resolving the EICS results in a similar distribution as what Getzlaff and
416 Dietze (2013) achieved with a simple parameterization of the EICS (Fig 9a). To compensate for the
417 “missing” EICS in coarse resolution models, they enhanced anisotropically the lateral diffusivity in
418 the equatorial region. Implementing this approach tends to homogenize oxygen levels zonally, with
419 an increase of the mean levels by 30-50 mmol.m⁻³ in the eastern basin and a decrease of oxygen
420 concentrations in the western basin.

421

422 A possibly not intuitive feature is that the oxygen levels are relatively similar in GFDL025 and
423 GFDL1, while the current system is relatively similar in GFDL025 and GFDL01 (see Fig 5 and Fig
424 9). An explanation lies in the relatively small net balance between large fluxes of respiration and
425 oxygen supply (Duteil et al., 2014). If the supply is slightly higher compared to the consumption by
426 respiration, it will lead to an increase of oxygen concentration. If it is slightly lower, the oxygen
427 levels will decrease. A small difference in supply (e.g slightly weaker currents) may therefore lead
428 to a large difference in oxygen levels when integrated over decades. For this reason, the impact of
429 the EICS is more visible below 1000 m as the respiration decreases following a power-law with
430 depth (Martin et al., 1987) and is therefore easier to offset even by a moderate oxygen supply.

431

432 **5. Summary and conclusions**

433 Intermediate water masses (IWM) are subducted in the Southern Ocean and transported
434 equatorward to the tropics by isopycnal processes (Sloyan and Kamenskovich, 2007; Sallee et al.,
435 2013; Meijers, 2014). At lower latitudes they recirculate into the lower thermocline of the tropical
436 regions at 500 - 1500 m and into the EICS (Zenk et al., 2005; Marin et al., 2010; Cravatte et al.,

437 2012; 2017; Ascani et al., 2015; Menesguen et al., 2019) (see schema Fig 1). We show here that the
438 representation of this ventilation pathway is important to take into account when assessing tropical
439 oxygen levels and the extent of the OMZ in coupled biogeochemical circulation or climate models.
440 Particularly, we highlight two critical, yet typical, biases that hamper the correct representation of
441 the tropical oxygen levels.

442

443 5.1 Subducted IWM properties and tropical oxygen

444 First, the current generation of climate models, such as the CMIP5 models, show large deficiencies
445 in simulating IWM. Along with an unrealistic representation of IWM volume and properties when
446 the waters enter the subtropics, the models also lack the observed prominent oxygen maximum
447 associated with IWM. Restoring oxygen levels to observed concentrations at 30°S/30°N and at
448 1500 m depth in a coarse resolution model, comparable to CMIP5 climate models in terms of
449 resolution and oxygen bias, shows a significant impact on the lower thermocline (500 – 1500 m)
450 oxygen levels : a positive anomaly of 60 mmol.m⁻³ translates into an oxygen increase by 10 mmol-
451 m⁻³ in tropical regions after 50 years of integration.

452

453 The equatorward transport of the anomaly in the subtropics is mostly due to isopycnal subgrid scale
454 mixing processes as shown by the NEMO2 budget analysis. While the models with differing ocean
455 resolutions may differ in their transport of IWM between the subtropical regions and the tropics, it
456 nevertheless suggests that mesoscale activity in higher resolution models is important to spread
457 IWM (e.g Xu et al., 2016). This possibly includes subsurface eddies that show a signature well into
458 the IWM depth range (Frenger et al., 2018, see their Fig 2).

459

460 5.2 IMW transport and Equatorial Intermediate Current System

461 Second, the Equatorial Intermediate Current System (EICS) is not represented in coarse resolution
462 models and only poorly represented in high resolution ocean circulation models (0.25° and 0.1°), as
463 its strength remains too weak by a factor of two (consistent with previous studies, e.g Ascani et al.,
464 2015). The EICS transports the IWM that occupies the lower thermocline (500 – 1500 m depth) and
465 the recirculation of the IWM in the tropical ocean, as suggested by the observational study of Zenk
466 et al. (2005), and shown in our study.

467

468 We investigated the impact of the EICS on the oxygen supply with tracer release experiments: the
469 concentration of a conservative tracer that originates from the subtropical ocean, is, after 50 years,
470 30 % higher in the eastern equatorial (5°N-5S) Pacific in an ocean model with 0.1° resolution,

471 compared to an ocean model with 0.5 ° resolution. As the oxygen gradient along the equator is
472 similar to the gradient of the conservative tracer, we assume a similar enhancement of oxygen
473 supply by 30 % in the eastern equatorial Pacific at the same time scale. This means, if we account
474 for oxygen consumption due to respiration (about 1 mmol.m⁻³.yr⁻¹ between 5°N-5°S, see section
475 3.2), that the better resolved EICS in the higher resolution ocean leads roughly to higher
476 intermediate oxygen levels of 15 - 30 mmol.m⁻³ compared to the lower resolution ocean experiment
477 in a timescale of 50 years. Consistently, 0.1°-ocean GFDL01 model displays oxygen concentrations
478 larger by about 30 mmol.m⁻³ in the eastern equatorial lower thermocline (500-1500 m) compared to
479 the 1°-ocean GFDL1 configuration (with higher subtropical oxygen concentrations of IWM of 15
480 mmol.m⁻³ in GFDL01 at 30°S)

481

482 We would like to highlight two potential implications of our finding of the important role of the
483 EICS for the Pacific eastern tropical oxygen supply: i) First, we have shown that the intermediate
484 current system EICS is important for the connection between the western and eastern Pacific Ocean
485 at a decadal / multidecadal time scale. This suggests that the EICS modulates the mean state and the
486 variability of the tropical oxygen in the lower thermocline, and subsequently the whole water
487 column by upwelling of deep waters. ii) Second, we have found an enhancement of the connections
488 between equatorial deep ocean (> 2000 m) and lower thermocline in the high resolution model
489 compared to the lower resolution model. This result is consistent with the studies of Brandt et al.
490 (2011, 2012), who suggested, based on observational data and on an idealized model, that
491 Equatorial Deep Jets, part of the EICS (see Fig 1b), propagate their energy upward and impact the
492 upper ocean properties of the ocean, including their oxygen content. Taken this into account, we
493 hypothesize that the Pacific Deep Water has a larger role than previously thought in modulating the
494 intermediate and upper ocean properties.

495

496 A pragmatic approach to account for the missing EICS is to increase diffusion anisotropically, with
497 increased zonal mixing in the tropics (Getzlaff and Dietze, 2013). This parameterization mimics a
498 more vigorous EICS and improves the simulated shape of the OMZ in climate models. However,
499 the prominent bias of IWM in climate models, and therefore of the water masses entering the EICS
500 is not accounted for with this parameterization. Furthermore such a parameterization improves the
501 mean state but does not reproduce the variability of the EICS.

502

503 5.3 Implication for biogeochemical cycles

504 The IWM are important supplier of oxygen to the tropical oceans, but also of nutrients (Palter et al.,
505 2010) as well as anthropogenic carbon (e.g Kathiwala et al., 2012), which accumulates in mode and
506 intermediate waters of the Southern Ocean (Sabine et al., 2004; Resplandy et al., 2013). The
507 mechanisms that we discussed here may therefore play a role in ocean carbon climate feedbacks on
508 time scales of decades to a century.

509

510 Finally, this study suggests that changes of the properties of the IWM may contribute to the still
511 partly unexplained deoxygenation of 5 mmol.m^{-3} / decade occurring in the lower thermocline of the
512 equatorial eastern Pacific Ocean (Schmidtko et al., 2017; Oschlies et al., 2018). In addition to an
513 oxygen decrease in tropical regions, Schmidtko et al. (2017) showed a decrease of oxygen levels by
514 $2\text{-}5 \text{ mmol.m}^{-3}$ in the regions of formations of AAIW. Based on repeated cruise observations,
515 Panassa et al. (2018) highlighted an increase of the apparent oxygen utilization in the core of the
516 AAIW, related to a 5 % increase in nutrient concentrations from 1990 to 2014. The transport of this
517 modified AAIW, poorer in oxygen and richer in nutrients, toward the low latitudes both by small
518 scale processes (section 3) and at the equator by the EICS (section 4), may explain a significant part
519 of the occurring deoxygenation in the equatorial ocean. In complement to changes in the AAIW
520 properties, little is known about the variability and long term trend of the strength of the EICS, an
521 oceanic “bridge” between the western and the eastern part of the basin. A possible way forward
522 could be to perform idealized model experiments in high resolution configurations, aiming to assess
523 both the effect of the observed change in the AAIW properties and of a potential change of EICS
524 strength on oxygen levels.

525

526

527 **Data and code availability**

528 The code for the Nucleus for European Modeling of the Ocean (NEMO) is available at:
529 <https://www.nemo-ocean.eu/>. The code for the University of Victoria (UVIC) model is available
530 at :<http://terra.seos.uvic.ca/model/>. The Lagrangian particles ARIANE code is available at
531 <http://stockage.univ-brest.fr/~grima/Ariane/>. The Coordinated Ocean-ice Reference Experiments
532 (COREv2) dataset is available at: <https://data1.gfdl.noaa.gov/nomads/forms/core/COREv2.html>.
533 The experiments data is available on request.

534

535

536

537 **Authors contributions**

538 OD conceived the study, performed the NEMO model and ARIANE experiments and analyzed the
539 data. IF preprocessed and helped to analyze the GFDL data. JG preprocessed and helped to analyze
540 the UVIC data. All authors discussed the results and wrote the manuscript.

541

542 **Competing interest**

543 The authors declare that they have no conflict of interest.

544

545 **Acknowledgments**

546 This work is a contribution of the SFB754 “Climate-Biogeochemistry Interactions in the Tropical
547 Ocean”, supported by the Deutsche Forschungsgemeinschaft (DFG). The NEMO simulations were
548 performed at the North German Supercomputing Alliance (HLRN). We would like to thank Markus
549 Scheinert (research unit “Ocean Dynamics”, GEOMAR) for his technical support in compiling the
550 NEMO code and for providing the high resolution NEMO input files. We would like to thank
551 GFDL for producing the CM2-0 suite that involved a substantial commitment of computational
552 resources and data storage. J.G acknowledge support by the project "Reduced Complexity Models"
553 (supported by the Helmholtz Association of German Research Centres (HGF) – grant no. ZT-I-
554 0010)

555

556

557

558

559

560

561

562

563

564

565

566

567

568

569

571 **References**

- 572 Ascani, F., Firing, E., Dutrieux, P., McCreary, J. P., & Ishida, A. (2010). Deep Equatorial Ocean
573 Circulation Induced by a Forced–Dissipated Yanai Beam. *Journal of Physical Oceanography*, 40(5),
574 1118–1142. doi:10.1175/2010jpo4356.1
- 575 Ascani, F., Firing, E., McCreary, J. P., Brandt, P., & Greatbatch, R. J. (2015). The Deep Equatorial
576 Ocean Circulation in Wind-Forced Numerical Solutions. *Journal of Physical Oceanography*, 45(6),
577 1709–1734. doi:10.1175/jpo-d-14-0171.1
- 578 Bahl, A., Gnanadesikan, A., & Pradal, M. A. (2019). Variations in Ocean Deoxygenation Across
579 Earth System Models: Isolating the Role of Parameterized Lateral Mixing. *Global Biogeochemical*
580 *Cycles*, 33(6), 703–724. doi:10.1029/2018gb006121
- 581 Blanke, B., & Raynaud, S. (1997). Kinematics of the Pacific Equatorial Undercurrent: An Eulerian
582 and Lagrangian Approach from GCM Results. *Journal of Physical Oceanography*, 27(6), 1038–
583 1053. doi:10.1175/1520-0485(1997)027<1038:kotpeu>2.0.co;2
- 584 Brandt, P., Funk, A., Hormann, V., Dengler, M., Greatbatch, R. J., & Toole, J. M. (2011).
585 Interannual atmospheric variability forced by the deep equatorial Atlantic Ocean. *Nature*,
586 473(7348), 497–500. doi:10.1038/nature10013
- 587 Brandt, P., Greatbatch, R. J., Claus, M., Didwischus, S.-H., Hormann, V., Funk, A., ... Körtzinger,
588 A. (2012). Ventilation of the equatorial Atlantic by the equatorial deep jets. *Journal of Geophysical*
589 *Research: Oceans*, 117(C12), n/a–n/a. doi:10.1029/2012jc008118
- 590 Breitburg, D., Levin, L. A., Oschlies, A., Grégoire, M., Chavez, F. P., Conley, D. J., ... Zhang, J.
591 (2018). Declining oxygen in the global ocean and coastal waters. *Science*, 359(6371), eaam7240.
592 doi:10.1126/science.aam7240
- 593 Busecke, J. J. M., Resplandy, L., & Dunne, J. P. (2019). The Equatorial Undercurrent and the
594 Oxygen Minimum Zone in the Pacific. *Geophysical Research Letters*, 46(12), 6716–6725.
595 doi:10.1029/2019gl082692
- 596 Cabré, A., Marinov, I., Bernardello, R., & Bianchi, D. (2015). Oxygen minimum zones in the
597 tropical Pacific across CMIP5 models: mean state differences and climate change trends.
598 *Biogeosciences*, 12(18), 5429–5454. doi:10.5194/bg-12-5429-2015
- 599 Carrasco, C., Karstensen, J., & Farias, L. (2017). On the Nitrous Oxide Accumulation in
600 Intermediate Waters of the Eastern South Pacific Ocean. *Frontiers in Marine Science*, 4,
601 doi:10.3389/fmars.2017.00024

602 Cravatte, S., Kessler, W. S., & Marin, F. (2012). Intermediate Zonal Jets in the Tropical Pacific
603 Ocean Observed by Argo Floats. *Journal of Physical Oceanography*, 42(9), 1475–1485.
604 doi:10.1175/jpo-d-11-0206.1

605 Cravatte, S., Kestenare, E., Marin, F., Dutrieux, P., & Firing, E. (2017). Subthermocline and
606 Intermediate Zonal Currents in the Tropical Pacific Ocean: Paths and Vertical Structure. *Journal of*
607 *Physical Oceanography*, 47(9), 2305–2324. doi:10.1175/jpo-d-17-0043.1

608 Czeschel, R., Stramma, L., Schwarzkopf, F. U., Giese, B. S., Funk, A., and Karstensen, J. (2011),
609 Middepth circulation of the eastern tropical South Pacific and its link to the oxygen minimum zone,
610 *J. Geophys. Res.*, 116, C01015, doi:10.1029/2010JC006565

611 Delworth, T. L., Rosati, A., Anderson, W., Adcroft, A. J., Balaji, V., Benson, R., ... Zhang, R.
612 (2012). Simulated Climate and Climate Change in the GFDL CM2.5 High-Resolution Coupled
613 Climate Model. *Journal of Climate*, 25(8), 2755–2781. doi:10.1175/jcli-d-11-00316.1

614 Dietze, H., & Loeptien, U. (2013). Revisiting “nutrient trapping” in global coupled biogeochemical
615 ocean circulation models. *Global Biogeochemical Cycles*, 27(2), 265–284. doi:10.1002/gbc.20029

616 Dufour, C. O., Griffies, S. M., de Souza, G. F., Frenger, I., Morrison, A. K., Palter, J. B., ... Slater,
617 R. D. (2015). Role of Mesoscale Eddies in Cross-Frontal Transport of Heat and Biogeochemical
618 Tracers in the Southern Ocean. *Journal of Physical Oceanography*, 45(12), 3057–3081. doi:10.1175/
619 jpo-d-14-0240.1

620 Duteil, O., & Oschlies, A. (2011). Sensitivity of simulated extent and future evolution of marine
621 suboxia to mixing intensity. *Geophysical Research Letters*, 38(6), n/a–n/a.
622 doi:10.1029/2011gl046877

623 Duteil, O., Koeve, W., Oschlies, A., Aumont, O., Bianchi, D., Bopp, L., ... Segschneider, J. (2012).
624 Preformed and regenerated phosphate in ocean general circulation models: can right total
625 concentrations be wrong? *Biogeosciences*, 9(5), 1797–1807. doi:10.5194/bg-9-1797-2012

626 Duteil, O., Böning, C. W., & Oschlies, A. (2014). Variability in subtropical-tropical cells drives
627 oxygen levels in the tropical Pacific Ocean. *Geophysical Research Letters*, 41(24), 8926–8934.
628 doi:10.1002/2014gl061774

629 Duteil, O., Oschlies, A., & Böning, C. W. (2018). Pacific Decadal Oscillation and recent oxygen
630 decline in the eastern tropical Pacific Ocean. *Biogeosciences*, 15(23), 7111–7126. doi:10.5194/bg-
631 15-7111-2018

632 Duteil, O. (2019). Wind Synoptic Activity Increases Oxygen Levels in the Tropical Pacific Ocean.
633 *Geophysical Research Letters*, 46(5), 2715–2725. doi:10.1029/2018gl081041

634 Eden, C., & Dengler, M. (2008). Stacked jets in the deep equatorial Atlantic Ocean. *Journal of*
635 *Geophysical Research*, 113(C4). doi:10.1029/2007jc004298

636 Firing, E., Wijffels, S. E., & Hacker, P. (1998). Equatorial subthermocline currents across the
637 Pacific. *Journal of Geophysical Research: Oceans*, 103(C10), 21413–21423. doi:10.1029/98jc01944

638 Firing, E. (1987). Deep zonal currents in the central equatorial Pacific. *Journal of Marine Research*,
639 45(4), 791–812. doi:10.1357/002224087788327163

640 Frenger, I., Bianchi, D., Stührenberg, C., Oeschies, A., Dunne, J., Deutsch, C., ... Schütte, F.
641 (2018). Biogeochemical Role of Subsurface Coherent Eddies in the Ocean: Tracer Cannonballs,
642 Hypoxic Storms, and Microbial Stewpots? *Global Biogeochemical Cycles*, 32(2), 226–249.
643 doi:10.1002/2017gb005743

644 Galbraith, E. D., Dunne, J. P., Gnanadesikan, A., Slater, R. D., Sarmiento, J. L., Dufour, C. O., ...
645 Marvasti, S. S. (2015). Complex functionality with minimal computation: Promise and pitfalls of
646 reduced-tracer ocean biogeochemistry models. *Journal of Advances in Modeling Earth Systems*,
647 7(4), 2012–2028. doi:10.1002/2015ms000463

648 Getzlaff, J., & Dietze, H. (2013). Effects of increased isopycnal diffusivity mimicking the
649 unresolved equatorial intermediate current system in an earth system climate model. *Geophysical*
650 *Research Letters*, 40(10), 2166–2170. doi:10.1002/grl.50419

651 Gnanadesikan, A., Bianchi, D., & Pradal, M. (2013). Critical role for mesoscale eddy diffusion in
652 supplying oxygen to hypoxic ocean waters. *Geophysical Research Letters*, 40(19), 5194–5198.
653 doi:10.1002/grl.50998

654 Gouriou, Y., Delcroix, T., & Eldin, G. (2006). Upper and intermediate circulation in the western
655 equatorial Pacific Ocean in October 1999 and April 2000. *Geophysical Research Letters*, 33(10), n/
656 a–n/a. doi:10.1029/2006gl025941

657 Griffies, S. M., Winton, M., Anderson, W. G., Benson, R., Delworth, T. L., Dufour, C. O., ...
658 Zhang, R. (2015). Impacts on Ocean Heat from Transient Mesoscale Eddies in a Hierarchy of
659 Climate Models. *Journal of Climate*, 28(3), 952–977. doi:10.1175/jcli-d-14-00353.1

660 Iudicone, D., Rodgers, K. B., Schopp, R., & Madec, G. (2007). An Exchange Window for the
661 Injection of Antarctic Intermediate Water into the South Pacific. *Journal of Physical Oceanography*,
662 37(1), 31–49. doi:10.1175/jpo2985.1

663 Izumo, T. (2005). The equatorial undercurrent, meridional overturning circulation, and their roles in
664 mass and heat exchanges during El Niño events in the tropical Pacific ocean. *Ocean Dynamics*,
665 55(2), 110–123. doi:10.1007/s10236-005-0115-1

666 Khatiwala, S., Tanhua, T., Mikaloff Fletcher, S., Gerber, M., Doney, S. C., Graven, H. D., ...
667 Sabine, C. L. (2013). Global ocean storage of anthropogenic carbon. *Biogeosciences*, 10(4), 2169–
668 2191. doi:10.5194/bg-10-2169-2013

669 Kawabe, M., & Fujio, S. (2010). Pacific ocean circulation based on observation. *Journal of*
670 *Oceanography*, 66(3), 389–403. doi:10.1007/s10872-010-0034-8

671 Keller, D. P., Oschlies, A., & Eby, M. (2012). A new marine ecosystem model for the University of
672 Victoria Earth System Climate Model. *Geoscientific Model Development*, 5(5), 1195–1220.
673 doi:10.5194/gmd-5-1195-2012

674 Koshlyakov, M.N. and Tarakanov, R.Y. (2003). Antarctic Bottom Water in the Pacific sector of the
675 Southern Ocean, *Oceanology* 43(1):1-15

676 Kriest, I., Khatiwala, S., & Oschlies, A. (2010). Towards an assessment of simple global marine
677 biogeochemical models of different complexity. *Progress in Oceanography*, 86(3-4), 337–360.
678 doi:10.1016/j.pocean.2010.05.002

679 Lachkar, Z., Orr, J. C., & Dutay, J.-C. (2009). Seasonal and mesoscale variability of oceanic
680 transport of anthropogenic CO₂. *Biogeosciences*, 6(11), 2509–2523. doi:10.5194/bg-6-2509-2009

681 Large, W. G., & Yeager, S. G. (2008). The global climatology of an interannually varying air–sea
682 flux data set. *Climate Dynamics*, 33(2-3), 341–364. doi:10.1007/s00382-008-0441-3

683 Lübbecke, J. F., Böning, C. W., & Biastoch, A. (2008). Variability in the subtropical-tropical cells
684 and its effect on near-surface temperature of the equatorial Pacific: a model study. *Ocean Science*,
685 4(1), 73–88. doi:10.5194/os-4-73-2008

686 Madec, G., Bourdallé-Badie, R., Pierre-Antoine Bouttier, Bricaud, C., Bruciaferri, D., Calvert, D.,
687 Chanut, J., Clementi, E., Coward, A., Delrosso, D., Ethé, C., Flavoni, S., Graham, T., Harle, J.,
688 Iovino, D., Lea, D., Lévy, C., Lovato, T., Martin, N., ... Vancoppenolle, M. (2017). NEMO ocean
689 engine. <https://doi.org/10.5281/ZENODO.3248739> Marin, F., Kestenare, E., Delcroix, T., Durand,
690 F., Cravatte, S., Eldin, G., & Bourdallé-Badie, R. (2010). Annual Reversal of the Equatorial
691 Intermediate Current in the Pacific: Observations and Model Diagnostics. *Journal of Physical*
692 *Oceanography*, 40(5), 915–933. doi:10.1175/2009jpo4318.1

693 Martin, J. H., Knauer, G. A., Karl, D. M., & Broenkow, W. W. (1987). VERTEX: carbon cycling in
694 the northeast Pacific. *Deep Sea Research Part A. Oceanographic Research Papers*, 34(2), 267–285.
695 doi:10.1016/0198-0149(87)90086-0

696 Meijers, A. J. S. (2014). The Southern Ocean in the Coupled Model Intercomparison Project phase
697 5. *Philosophical Transactions of the Royal Society A: Mathematical, Physical and Engineering*
698 *Sciences*, 372(2019), 20130296. doi:10.1098/rsta.2013.0296

699 Ménesguen, C., Delpech, A., Marin, F., Cravatte, S., Schopp, R., & Morel, Y. (2019). Observations
700 and Mechanisms for the Formation of Deep Equatorial and Tropical Circulation. *Earth and Space*
701 *Science*, 6(3), 370–386. doi:10.1029/2018ea000438

702 Molinelli EJ (1981) The Antarctic influence on Antarctic Intermediate Water. *J Mar Res* 39:267–
703 293

704 Oschlies, A., Brandt, P., Stramma, L., & Schmidtko, S. (2018). Drivers and mechanisms of ocean
705 deoxygenation. *Nature Geoscience*, 11(7), 467–473. doi:10.1038/s41561-018-0152-2

706 Palter, J. B., Sarmiento, J. L., Gnanadesikan, A., Simeon, J., and Slater, R. D. (2010). Fueling
707 export production: nutrient return pathways from the deep ocean and their dependence on the
708 Meridional Overturning Circulation, *Biogeosciences*, 7, 3549–3568, doi:10.5194/bg-7-3549-2010

709 Panassa, E., Santana-Casiano, J. M., González-Dávila, M., Hoppema, M., van Heuven, S. M. A. .,
710 Völker, C., ... Hauck, J. (2018). Variability of nutrients and carbon dioxide in the Antarctic
711 Intermediate Water between 1990 and 2014. *Ocean Dynamics*, 68(3), 295–308.
712 doi:10.1007/s10236-018-1131-2

713 Pardo, P. C., Pérez, F. F., Velo, A., & Gilcoto, M. (2012). Water masses distribution in the Southern
714 Ocean: Improvement of an extended OMP (eOMP) analysis. *Progress in Oceanography*, 103, 92–
715 105. doi:10.1016/j.pocean.2012.06.002

716 Paulmier, A., Ruiz-Pino (2009), D. Oxygen minimum zones (OMZs) in the modern ocean, *Progress*
717 *in Oceanography*, 80(3), 113-128, doi:10.1016/j.pocean.2008.08.001.

718 Qu, T., & Lindstrom, E. J. (2004). Northward Intrusion of Antarctic Intermediate Water in the
719 Western Pacific*. *Journal of Physical Oceanography*, 34(9), 2104–2118. doi:10.1175/1520-
720 0485(2004)034<2104:nioaiw>2.0.co;2

721 Resplandy, L., Bopp, L., Orr, J. C., & Dunne, J. P. (2013). Role of mode and intermediate waters in
722 future ocean acidification: Analysis of CMIP5 models. *Geophysical Research Letters*, 40(12),
723 3091–3095. doi:10.1002/grl.50414

724 Rowe, G. D., Firing, E., & Johnson, G. C. (2000). Pacific Equatorial Subsurface Countercurrent
725 Velocity, Transport, and Potential Vorticity*. *Journal of Physical Oceanography*, 30(6), 1172–1187.
726 doi:10.1175/1520-0485(2000)030<1172:pescvt>2.0.co;2

727 Russell, J. L., & Dickson, A. G. (2003). Variability in oxygen and nutrients in South Pacific
728 Antarctic Intermediate Water. *Global Biogeochemical Cycles*, 17(2), n/a–n/a.
729 doi:10.1029/2000gb001317

730 Sabine, C. L. (2004). The Oceanic Sink for Anthropogenic CO₂. *Science*, 305(5682), 367–371.
731 doi:10.1126/science.1097403

732 Sallée, J.-B., Shuckburgh, E., Bruneau, N., Meijers, A. J. S., Bracegirdle, T. J., Wang, Z., & Roy, T.
733 (2013). Assessment of Southern Ocean water mass circulation and characteristics in CMIP5
734 models: Historical bias and forcing response. *Journal of Geophysical Research: Oceans*, 118(4),
735 1830–1844. doi:10.1002/jgrc.20135

736 Schmidtko, S., Stramma, L., & Visbeck, M. (2017). Decline in global oceanic oxygen content
737 during the past five decades. *Nature*, 542(7641), 335–339. doi:10.1038/nature21399

738 Sen Gupta, A., & England, M. H. (2007). Evaluation of Interior Circulation in a High-Resolution
739 Global Ocean Model. Part II: Southern Hemisphere Intermediate, Mode, and Thermocline Waters.
740 *Journal of Physical Oceanography*, 37(11), 2612–2636. doi:10.1175/2007jpo3644.1

741 Shigemitsu, M., Yamamoto, A., Oka, A., & Yamanaka, Y. (2017). One possible uncertainty in
742 CMIP5 projections of low-oxygen water volume in the Eastern Tropical Pacific. *Global
743 Biogeochemical Cycles*, 31(5), 804–820. doi:10.1002/2016gb005447

744 Sloyan, B. M., & Kamenkovich, I. V. (2007). Simulation of Subantarctic Mode and Antarctic
745 Intermediate Waters in Climate Models. *Journal of Climate*, 20(20), 5061–5080.
746 doi:10.1175/jcli4295.1

747 Sloyan, B. M., & Rintoul, S. R. (2001). Circulation, Renewal, and Modification of Antarctic Mode
748 and Intermediate Water*. *Journal of Physical Oceanography*, 31(4), 1005–1030. doi:10.1175/1520-
749 0485(2001)031<1005:cramoa>2.0.co;2

750 Takano, Y., Ito, T., & Deutsch, C. (2018). Projected Centennial Oxygen Trends and Their
751 Attribution to Distinct Ocean Climate Forcings. *Global Biogeochemical Cycles*, 32(9), 1329–1349.
752 doi:10.1029/2018gb005939

753 Talley, L. D. (1993). Distribution and Formation of North Pacific Intermediate Water. *Journal of
754 Physical Oceanography*, 23(3), 517–537. doi:10.1175/1520-0485(1993)023<0517:dafonp>2.0.co;2

755 Weaver, A. J., Eby, M., Wiebe, E. C., Bitz, C. M., Duffy, P. B., Ewen, T. L., ... Yoshimori, M.
756 (2001). The UVic earth system climate model: Model description, climatology, and applications to
757 past, present and future climates. *Atmosphere-Ocean*, 39(4), 361–428.
758 doi:10.1080/07055900.2001.9649686

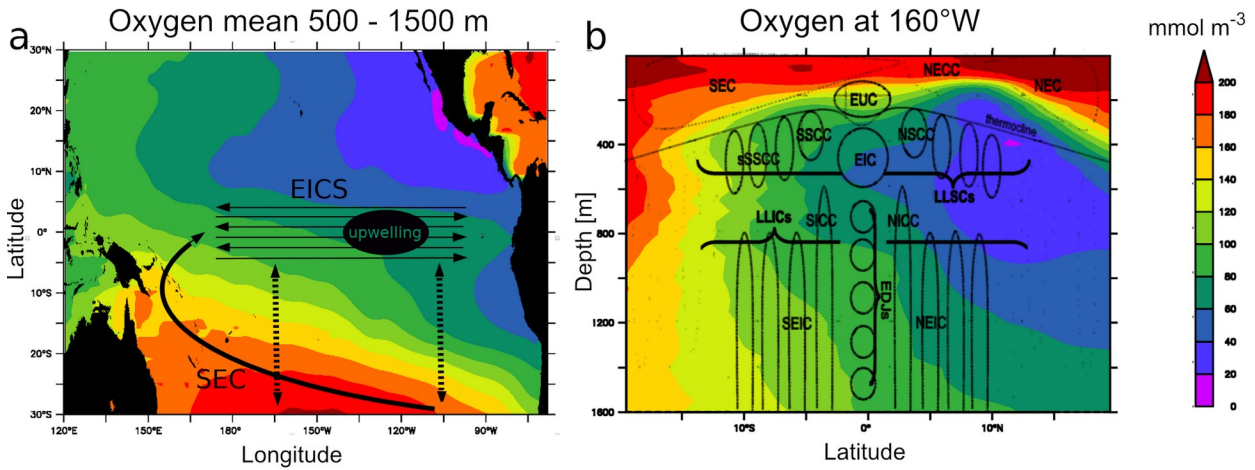
759 Xu, L., Li, P., Xie, S. et al. (2016). Observing mesoscale eddy effects on mode-water subduction
760 and transport in the North Pacific. *Nature Communications*, 10505 (2016),
761 doi.org/10.1038/ncomms10505

762 Zenk, W., Siedler, G., Ishida, A., Holfort, J., Kashino, Y., Kuroda, Y., ... Müller, T. J. (2005).
763 Pathways and variability of the Antarctic Intermediate Water in the western equatorial Pacific
764 Ocean. *Progress in Oceanography*, 67(1-2), 245–281. doi:10.1016/j.pocean.2005.05.003

765 Zhu, C., Liu, Z., & Gu, S. (2017). Model bias for South Atlantic Antarctic intermediate water in
766 CMIP5. *Climate Dynamics*, 50(9-10), 3613–3624. doi:10.1007/s00382-017-3828-1

767
768
769

770 **Figures and Table**



771

772

773 Figure 1 : a- schema summarizing the intermediate water masses (IWM) pathway from the
774 subtropics into the equatorial regions. EICS : Equatorial Intermediate Current System. SEC : South
775 Equatorial Current. Dashed line : isopycnal diffusive processes. Observed (World Ocean Atlas)
776 oxygen levels (mmol.m^{-3}) in the lower thermocline (mean 500-1500m) are represented in color. b -
777 schema (adapted from Menesguen et al., 2019) illustrating the complexity of the EICS, extending
778 below the thermocline till more than 2000 m depth (see section 4.1 for a detailed description).
779 Observed (World Ocean Atlas) oxygen levels at 160°W are represented in color.

780

781

782

783

784

785

786

787

788

789

790

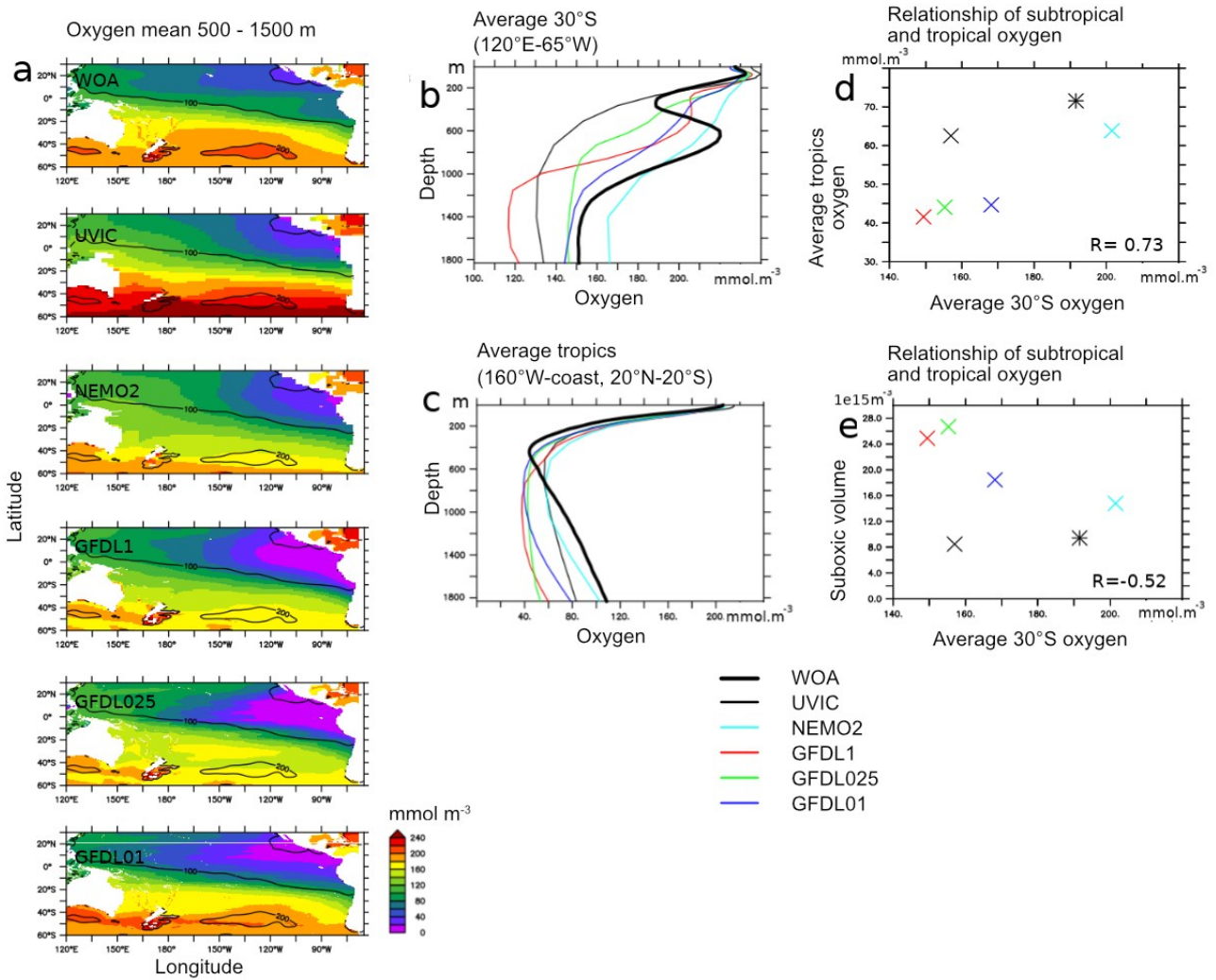
791

792

793

794

795



797

798 Figure 2 : a- oxygen levels (mmol.m⁻³) in observations (World Ocean Atlas - WOA) (mean 500 –
 799 1500 m) and models (UVIC, NEMO2, GFDL1, GFDL025, GFDL01). Contours correspond to
 800 WOA values. b: average “30°S” (120°E-65°W, 30°S) c : average “tropics” (160°W-coast, 20°N-
 801 20°S). d: average “30°S” vs “tropics”. e: average “30°S” vs volume of tropical suboxic ocean
 802 (oxygen lower than 20 mmol.m⁻³) regions (1e15m³). b-e : UVIC : black, NEMO2 : cyan, GFDL1 :
 803 red, GFDL025, green; GFDL01 : blue, WOA: bold line (b,c) and star (d,e).

804

805

806

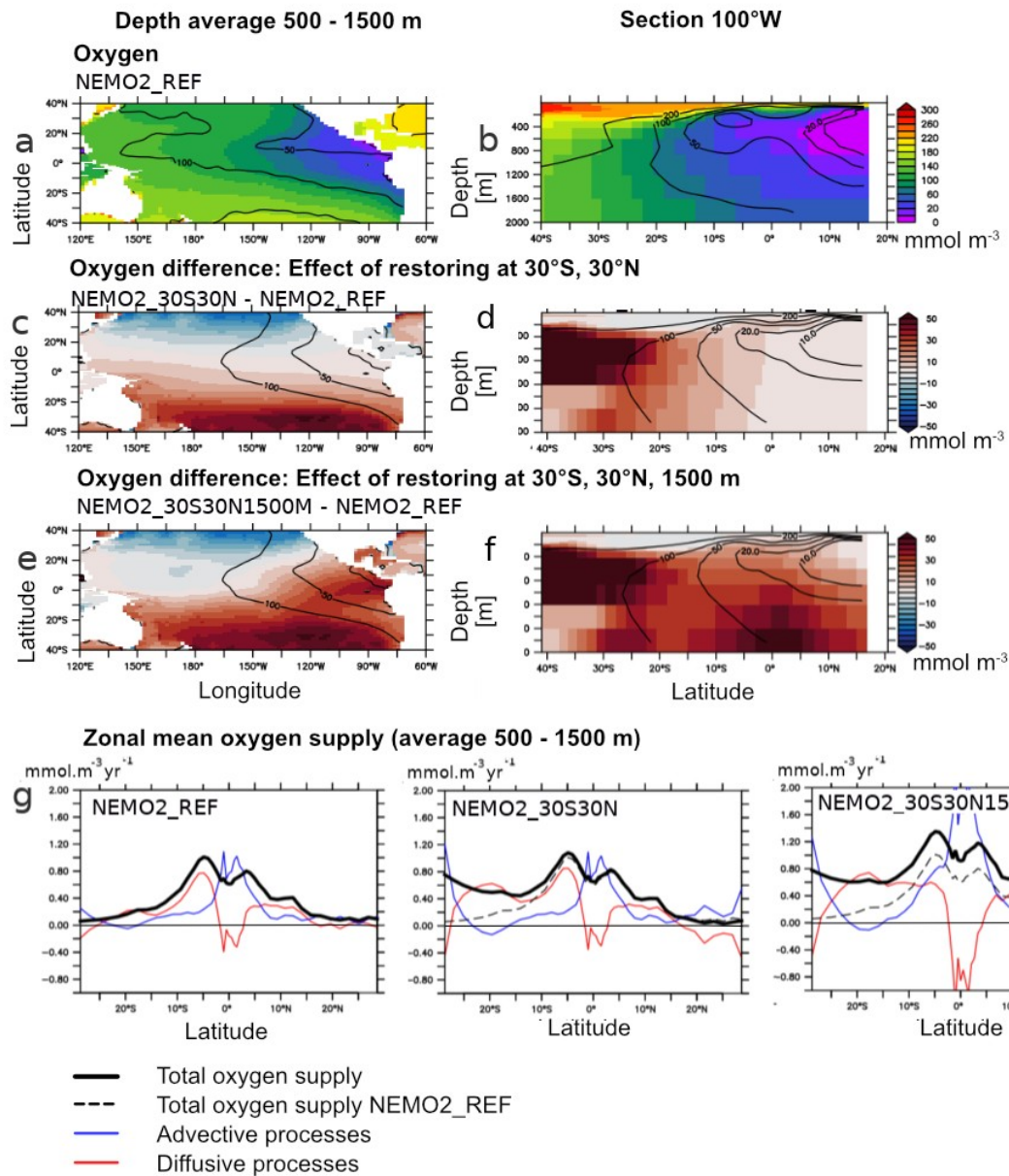
807

808

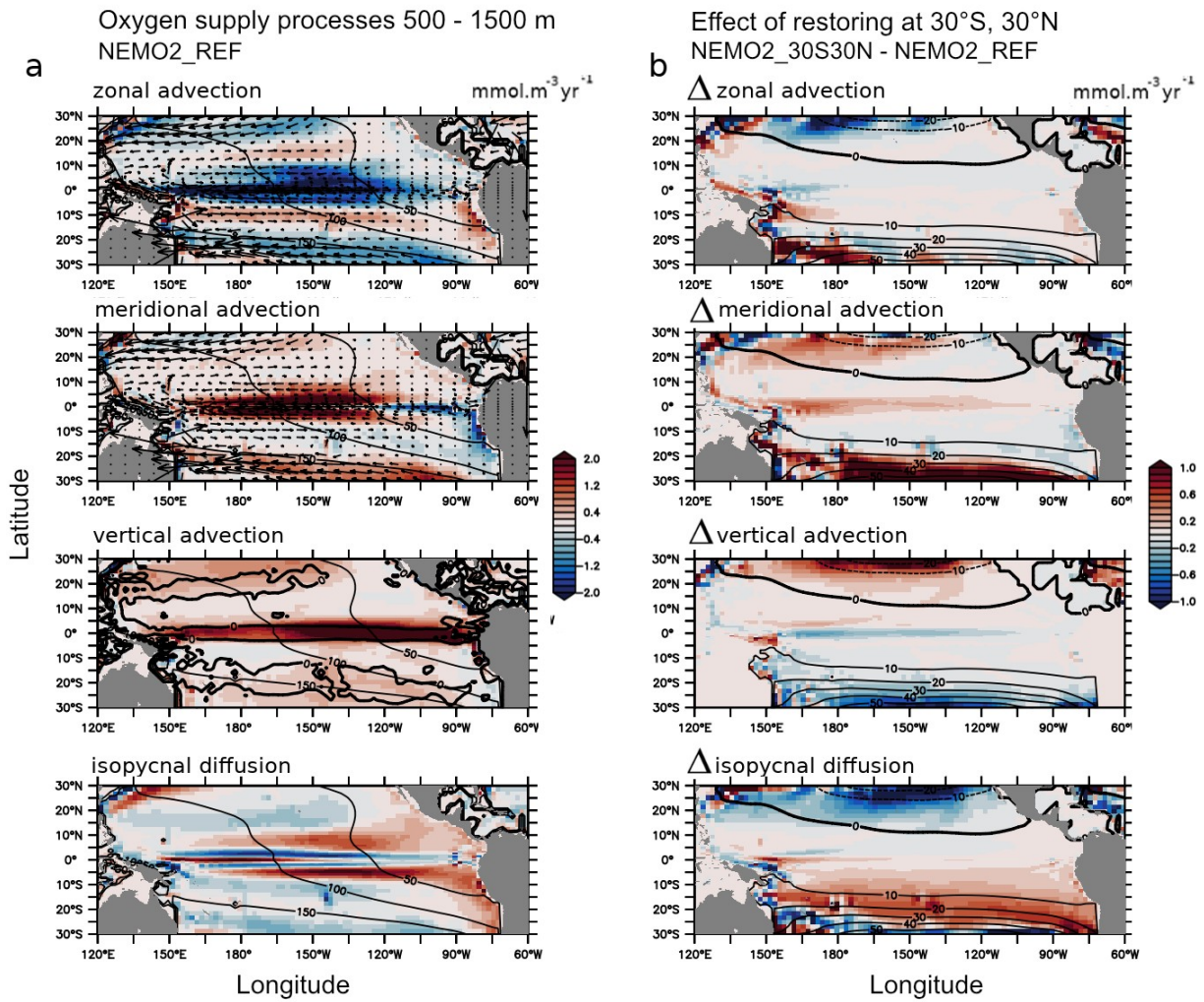
809

810

811



814 Figure 3 : a,b: Oxygen (mmol.m^{-3}) in the experiments NEMO2_REF (color) and World Ocean Atlas
 815 (contour) (a- average 500-1500 m, b- 100°W). c,d: Oxygen (mmol.m^{-3}) difference (c- average 500 –
 816 1500m, d- 100°W) between the experiments NEMO2_30S30N minus NEMO2_REF. e,f : Oxygen
 817 (mmol.m^{-3}) difference (e- average 500-1500m, f- 100°W) between the experiments
 818 NEMO2_30S30N1500M minus NEMO2_REF. g- basin zonal average (average 500 - 1500 m) of
 819 the oxygen total supply (bold) ($\text{mmol.m}^{-3}.\text{year}^{-1}$), advective processes (blue) and isopycnal diffusion
 820 (red) in NEMO2_REF, NEMO2_30S30N, NEMO2_30S30N1500M. The dashed line is the oxygen
 821 total supply in NEMO2_REF.



824 Figure 4 : a- Oxygen supply processes ($\text{mmol.m}^{-3}\text{.year}^{-1}$ – average 500 - 1500m) in NEMO2_REF :
 825 zonal advection, meridional advection, vertical advection, isopycnal diffusion. The mean meridional
 826 and zonal currents are displayed as vectors (meridional, zonal advection). The mean vertical current
 827 (0 isoline) is represented as bold contour (vertical advection). Oxygen levels (mmol.m^{-3}) are
 828 displayed in black contour. b- Difference in oxygen supply processes ($\text{mmol.m}^{-3}\text{.year}^{-1}$ – average
 829 500-1500m) between NEMO2_30S30N and NEMO2_REF : zonal advection, meridional advection,
 830 vertical advection, isopycnal diffusion. The NEMO2_30S30N – NEMO2_REF oxygen anomaly
 831 (mmol.m^{-3}) is displayed in contour.

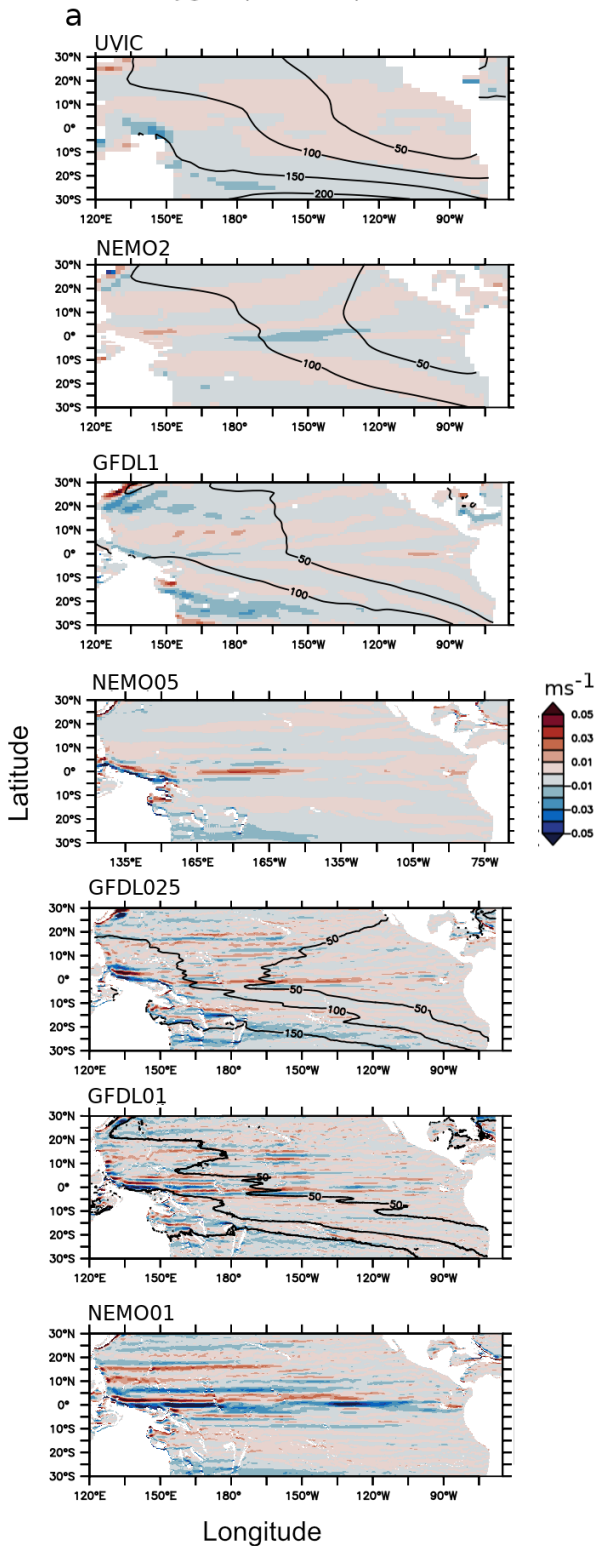
832

833

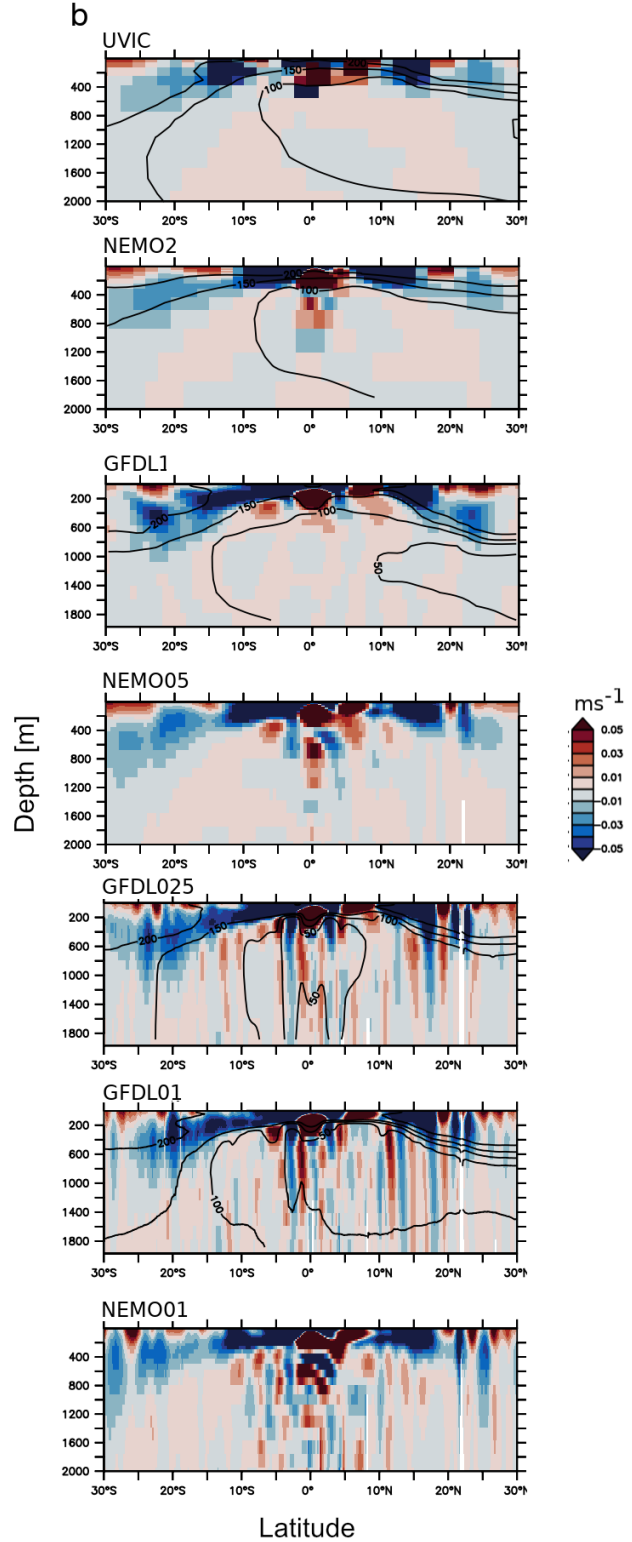
834

835

Zonal velocity component at 1000 m (colors) and oxygen (contours)

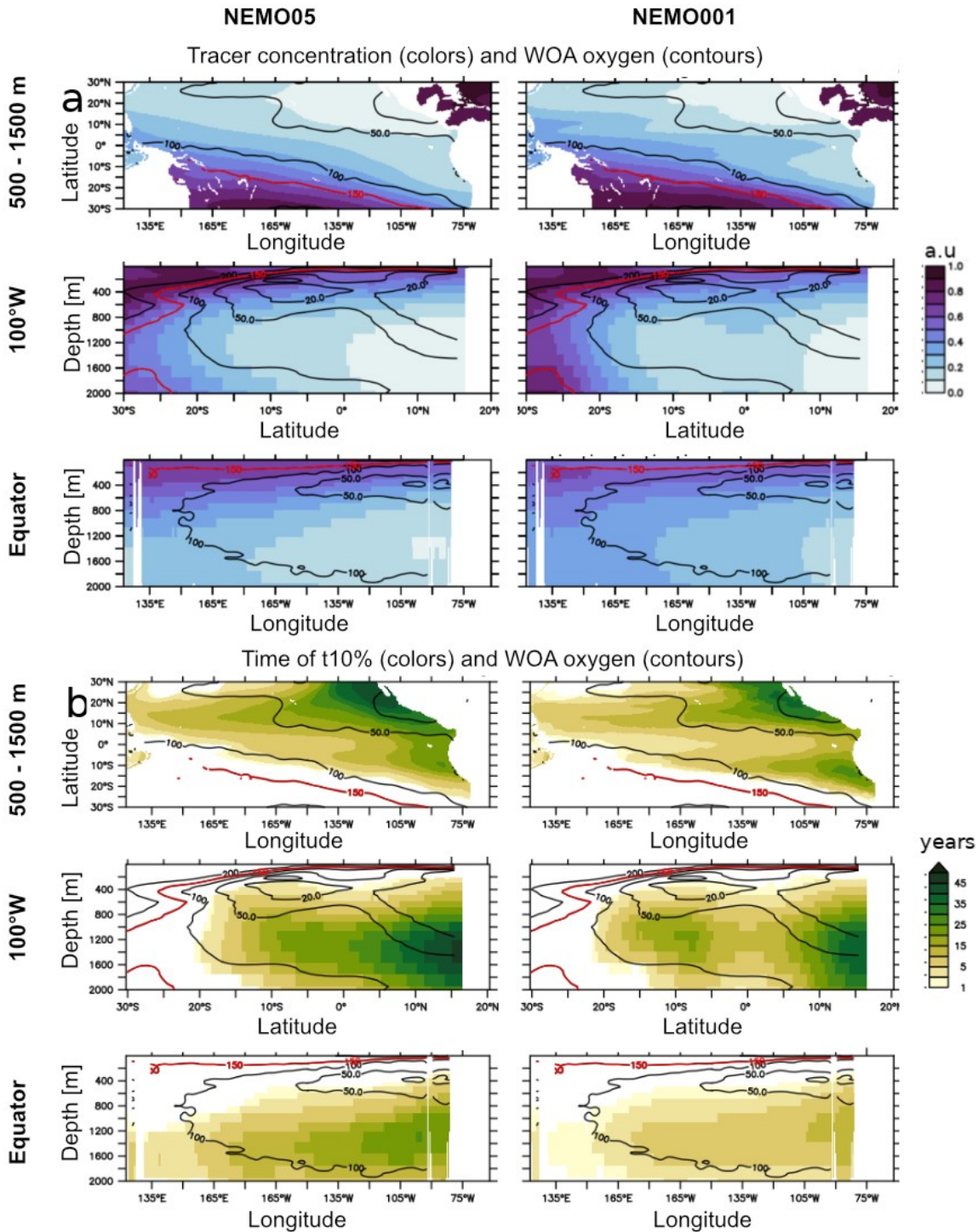


Zonal velocity component at 100°W (colors) and oxygen (contours)



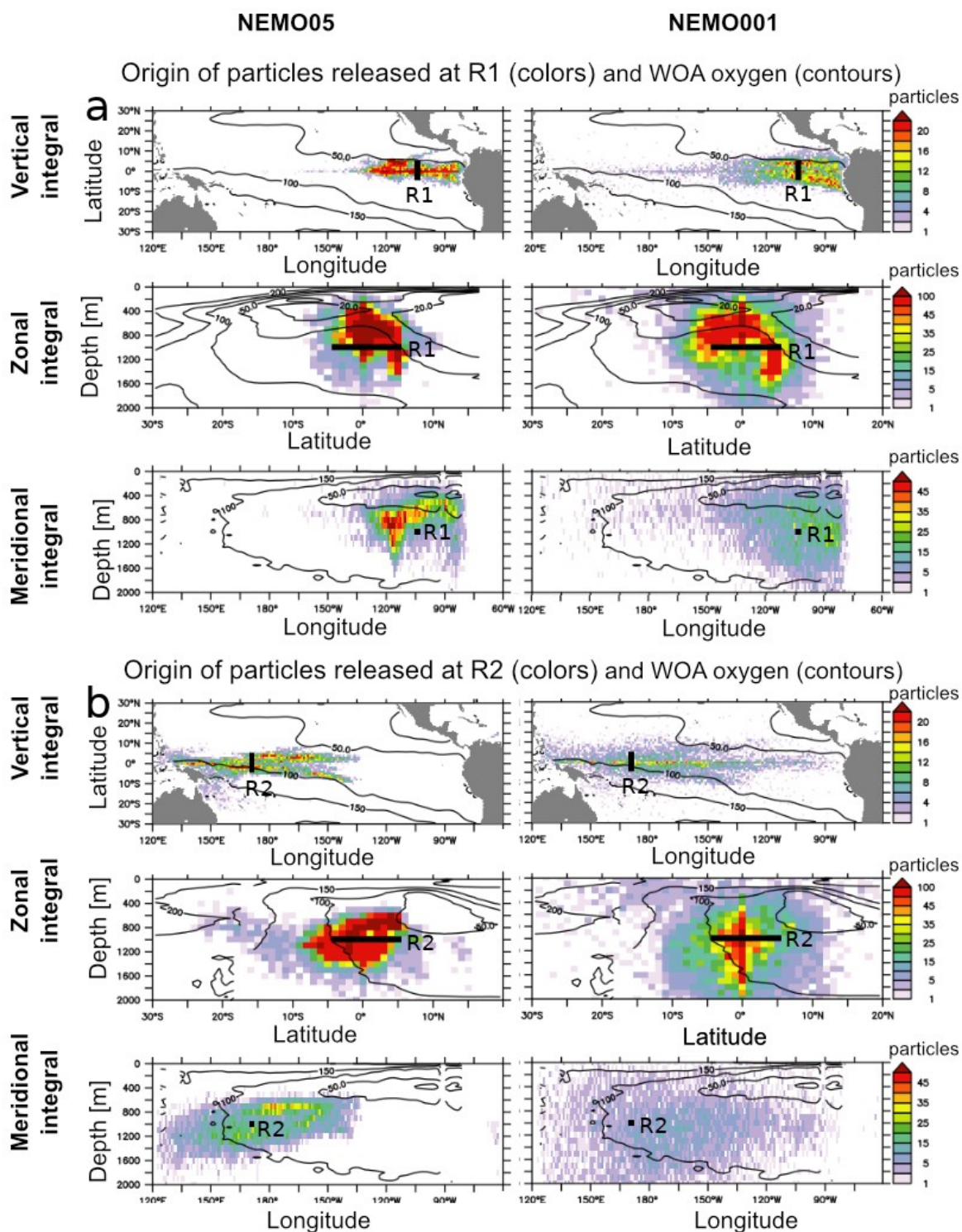
836

837 Figure 5 : mean currents velocity (ms⁻¹) at a- 1000 m depth b- 100°W in UVIC, NEMO2,
 838 NEMO05, GFDL025, GFDL01, NEMO01. The mean oxygen levels (mmol.m⁻³) (when coupled
 839 circulation-biogeochemical experiments have been performed – see Table 1) are displayed in
 840 contour



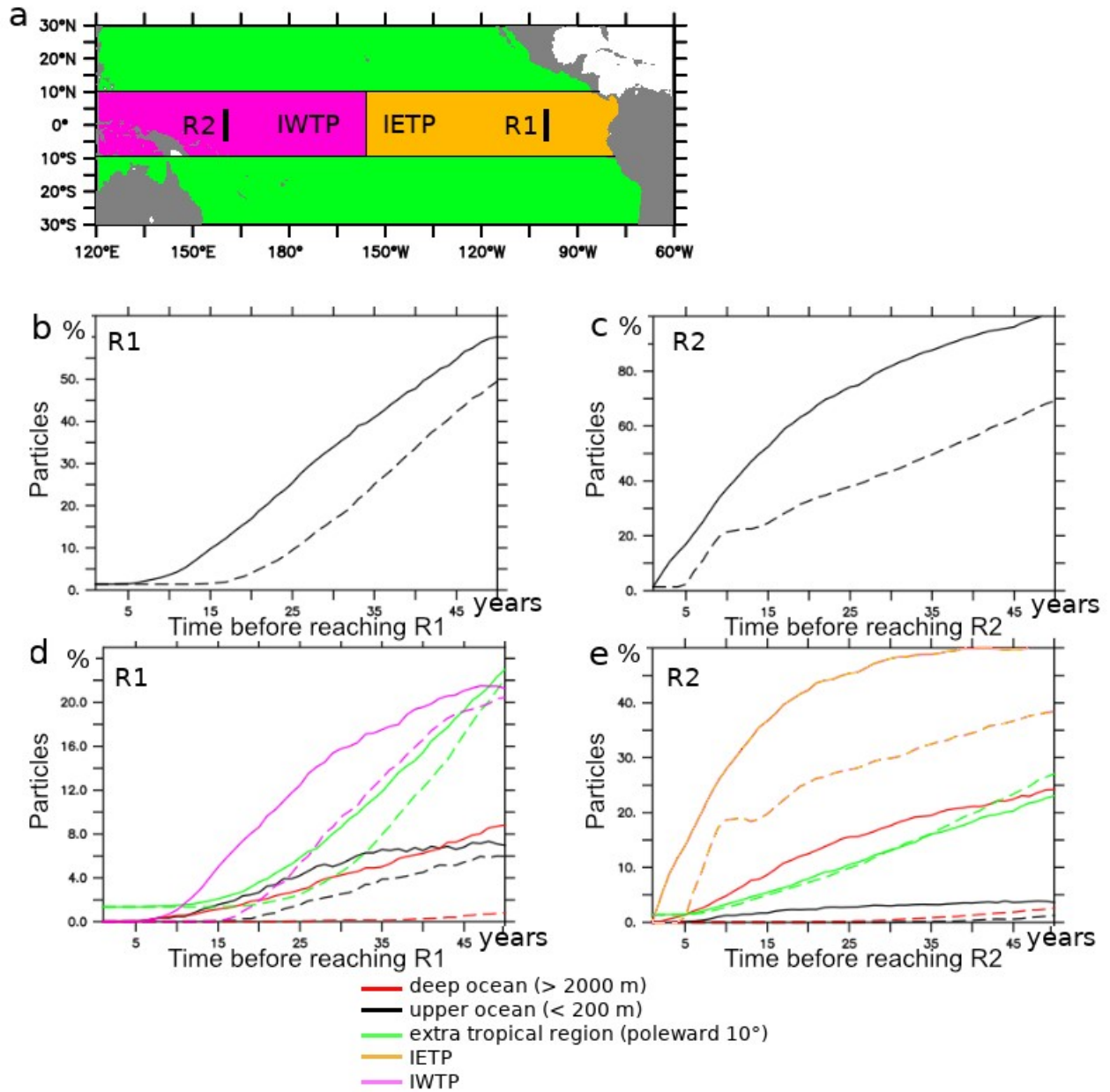
842

843 Figure 6: a : tracer concentration (arbitrary unit) after 60 years integration in NEMO05 and
 844 NEMO01: average 500-1500m, section 100°W, equatorial section. b: Time (years) at which the
 845 released tracer reaches the concentration 0.1 (t10%) in NEMO05 and NEMO01: average 500-
 846 1500m, section 100°W, equatorial section. In all the subpanels, the WOA oxygen levels are
 847 displayed in contour. The red contour is the WOA 150 mmol.m^{-3} oxygen isoline, used to initialize
 848 the tracer level.



849

850 Figure 7 : Density (number of particles in a $1^\circ \times 1^\circ \times 100\text{m}$ depth box) distribution of the location of
 851 released Lagrangian particles (15 years backward integration starting from the final experiment
 852 state) in NEMO05 and NEMO01. The release location is identified in bold and is located a- at
 853 $100^\circ\text{W}/5^\circ\text{N}-5^\circ\text{S}/1000$ m depth (R1). b- at $160^\circ\text{E}/5^\circ\text{N}-5^\circ\text{S}/1000$ m depth (R2). The particles have
 854 been integrated vertically, zonally and meridionally. The observed mean oxygen levels (WOA) are
 855 displayed in contour.



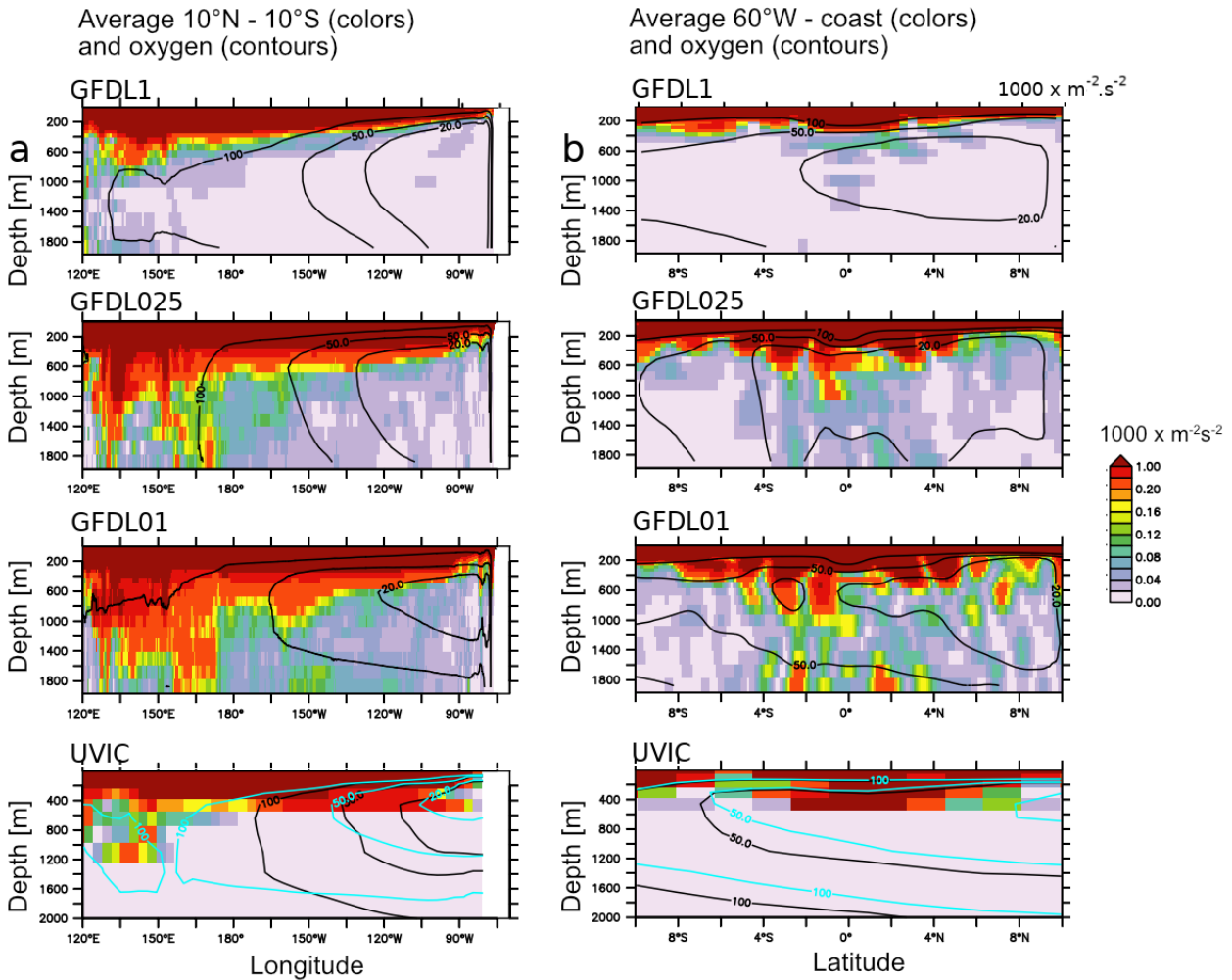
857

858

859 Figure 8 : a- schema summarizing the releases (R1: 100°W / 5°N-5°S / 1000 m , R2: 160°E /
 860 5N°5S / 1000 m) location, the IETP (Intermediate Eastern Tropical Pacific), IWTP (Intermediate
 861 Western Tropical Pacific) regional extension. b. percentage of particles (release R1) originating
 862 from outside the IETP ocean region. b- percentage of particles (release R2) originating from outside
 863 the IWTP ocean region. d- percentage of particles (release R1) originating from the upper ocean
 864 (shallower than 200 m), the deeper ocean (deeper than 2000 m), subtropical regions (poleward 10°),
 865 the IWTP. e- percentage of particles (release R2) originating from the upper ocean (shallower than
 866 200 m), the deeper ocean (deeper than 2000 m), subtropical regions (poleward 10°), the IETP.

867

Mean kinetic energy



869

870

871 Figure 9 : a - Mean Kinetic Energy ($m^2.s^{-2} \times 1000$) (average $10^\circ N-10^\circ S$) in GFDL01, GFDL025,
 872 GFDL01, UVIC, b - similar to a. but average $160^\circ W$ - coast. Oxygen levels ($mmol.m^{-3}$) are
 873 displayed in black contour. The blue contour corresponds to UVIC GD13 (Getzlaff and Dietze,
 874 2013, including an anisotropical increase of lateral diffusion at the equator)

875

876

877

878

879

880

881

882

883 Table 1 :

Model	Resolution	Atmosphere	Integration (years)	BGC	Model Reference (circulation)	Model Reference (BGC)
Mean state comparison						
UVIC	2.8°	Coupled (temperature, humidity) Forced (NCEP/NCAR wind stress)	10000	UVIC-BGC	Weaver et al., 2001	Keller et al., 2012
NEMO2	2° (0.5 eq)	Forced COREv2 “normal year”	1000	NPZD-O2	Madec et al., 2015	Kriest et al., 2010 Duteil et al., 2014
GFDL1	1°	Coupled	190	BLING	Delworth et al., 2012, Griffies et al., 2015	Galbraith et al., 2015
GFDL025	0.25°	Coupled	190	BLING		
GFDL01	0.1°	Coupled	190	BLING		
Process oriented experiments						
Model	Resolution	Atmosphere	Integration (years)	BGC	Characteristics	
NEMO2-REF -30N30S -30N30S1500M (section 2.2.1)	2° (0.5 eq)	Forced COREv2 1948-2007	60	NPZD-O2	- control experiment - O2 restoring to WOA at 30°N/30°S - O2 restoring to WOA at 30°N/30°S/1500m	
NEMO05 (section 2.2.2)	0.5°	Forced COREv2 1948 - 2007	60	Tracer release	- Tracer initialized to 1 (O2 WOA > 150 mmol.m-3) or 0 (O2 WOA < 150 mmol-m-3)	
NEMO01 (section 2.2.2)	0.1°	Forced COREv2 1948 – 2007	60	Tracer release		

884

885

886

887

888

889

890

891 **Appendix A**

892

893 The differences in oxygen levels between the “models groups” (GFDL suite, UVIC, NEMO2) are
894 partly related to differences in the atmospheric fields employed and the integration time (see 2).

895

896 1. Wind forcing

897 Zonal wind mean stress typically vary by 5 to 20 % between the different wind products (Chauduri
898 et al., 2013). To test this impact, we performed an experiment using the UVIC model using 2
899 different wind products (NCEP and COREv2 – Large and Yeager, 2009) (Figure A1). While the
900 shape of the OMZ shows slight differences, the volume of the OMZ and the mean oxygen levels in
901 the tropical regions and in the mid latitudes are similar. Consistent with the Figure 2, higher oxygen
902 levels at 30°S lead to higher oxygen levels in the tropical ocean and to a smaller OMZ volume
903 (Figure A2)

904

905

906

907

908

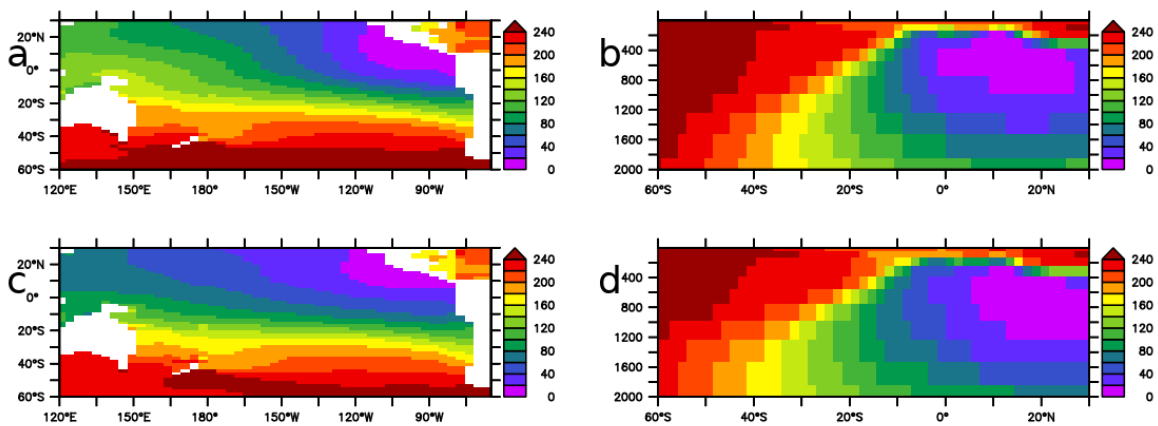
909

910

911

912

913



914 Figure A1 : Oxygen levels in UVIC (10000 years integration) a- mean 500-1500 m forcing NCEP.
915 b- section 120°W forcing NCEP. c- mean 500-1500 m forcing COREv2, d- section 120°W forcing
916 COREv2.

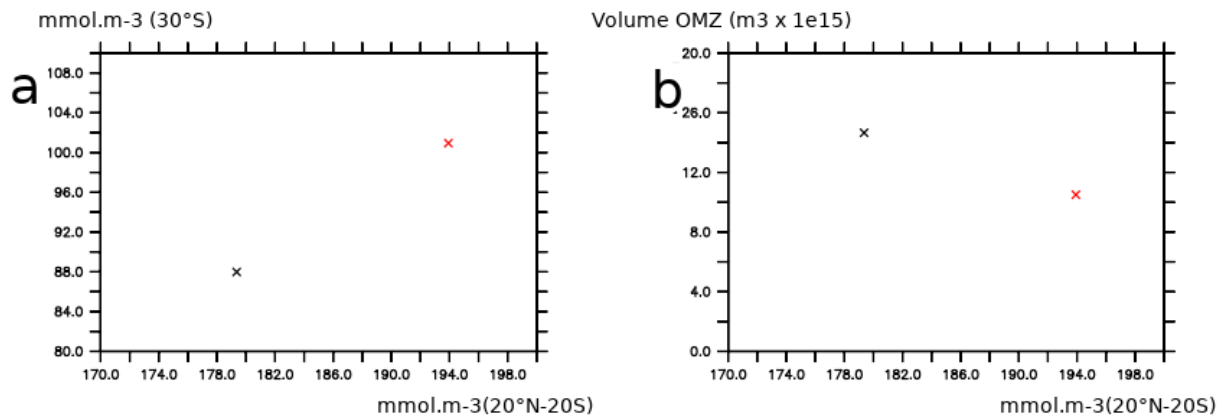
917

918

919

920

921



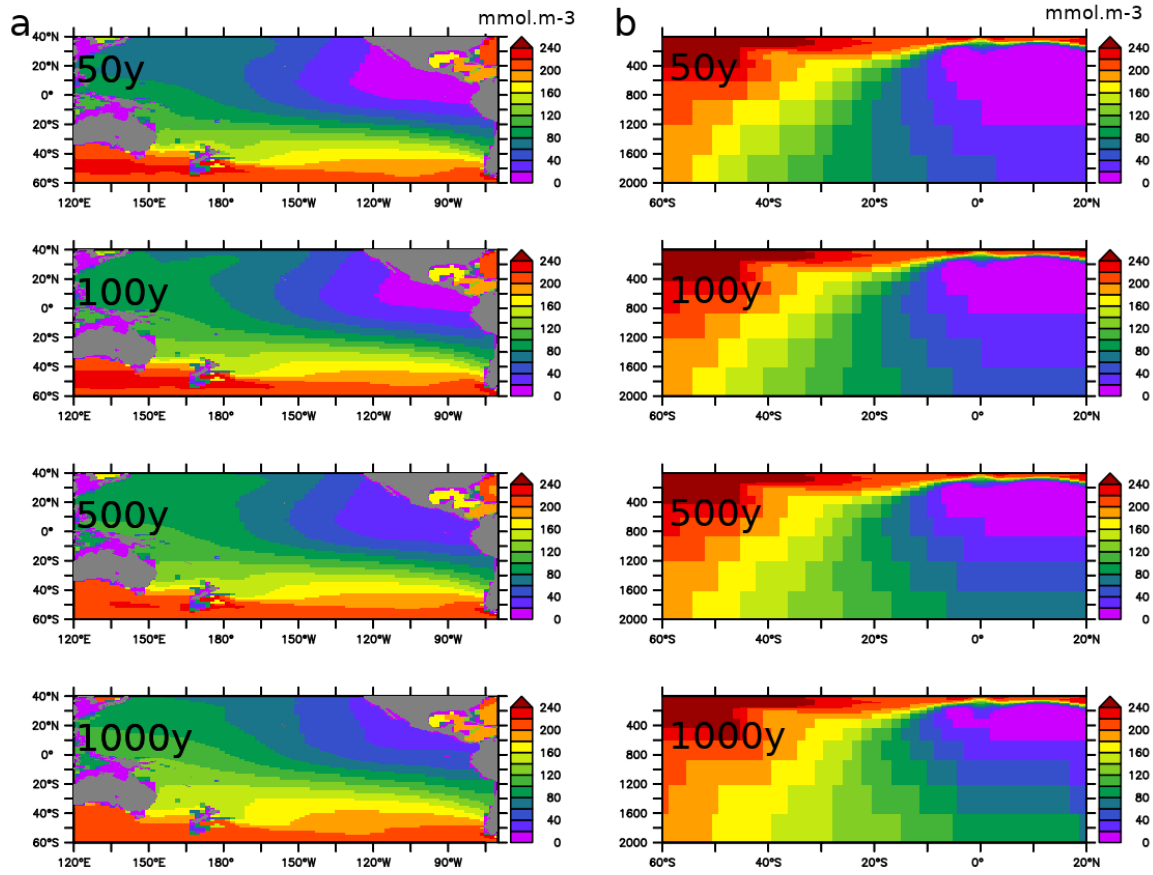
922 Figure A2 : a - Oxygen levels in UVIC (10000 years integration) at 30°S (zonal mean in the Pacific
 923 Ocean from surface to 2000 m depth) and in the tropical regions (20°S-20°N, averaged over the
 924 whole Pacific Ocean). b - Oxygen levels in UVIC (10000 years integration) at 30°S (zonal mean in
 925 the Pacific Ocean, from surface to 2000 m depth) and volume of the OMZ in the Pacific Ocean. The
 926 configuration forced by COREv2 is shown in black, the configuration forced by NCEP is shown in
 927 red.

928

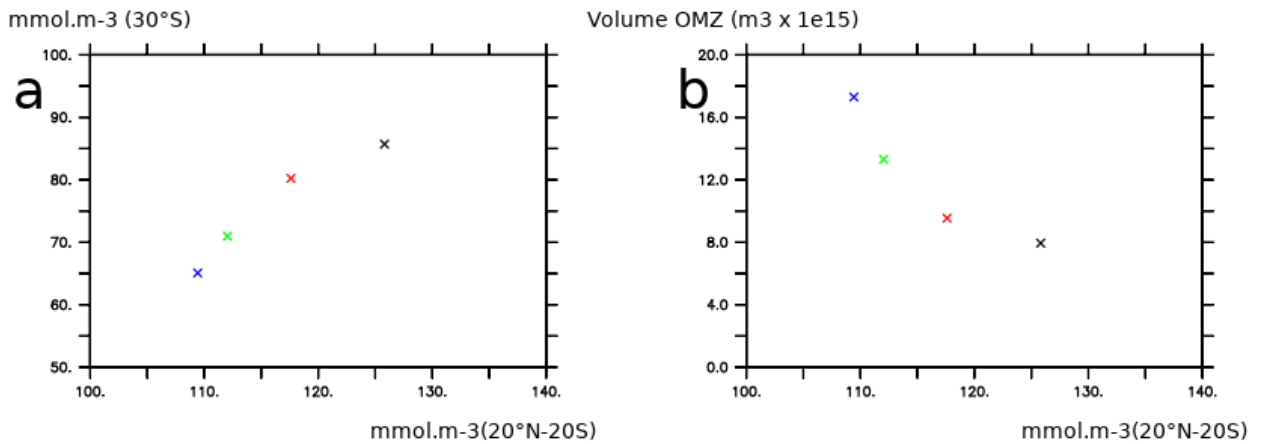
929 2. Spinup state

930 In complement, the spinup state of the model also impacts the oxygen levels as the deep ocean
 931 needs thousands of years to be in equilibrium. It may explain why UVIC (integrated for 10000
 932 years) is characterized by much larger oxygen levels than the GFDL model suite (integrated for 190
 933 years). As an example, the Figure A3 shows the evolution of oxygen levels during spinup in
 934 NEMO2. Larger oxygen levels at 30°S (e.g after 1000 years of integration) are characterized by a
 935 smaller OMZ volume (which is consistent with Fig 2) (Figure A4)

936



938 Figure A3 : oxygen levels at a - intermediate depth (average 500 – 2000 m) and b - 120°W in
 939 NEMO2 after 50, 100,500 and 1000 years integration



941 Figure A4 : a - Oxygen levels in NEMO2 at 30°S (zonal mean in the Pacific Ocean from surface to
 942 2000 m depth) and in the tropical regions (20°S-20°N, averaged over the whole Pacific Ocean from
 943 surface to 2000 m depth). b - Oxygen levels in NEMO2 at 30°S (zonal mean in the Pacific Ocean
 944 from surface to 2000 m depth) and volume of the OMZ in the Pacific Ocean. The color of the cross

945 depends of the integration duration (black : 50 years, red : 100 years, green : 500 years, blue 1000
946 years).

947

948

949

950 References

951 Chaudhuri, Ayan & Ponte, Rui & Forget, Gael & Heimbach, Patrick. (2013). A Comparison of
952 Atmospheric Reanalysis Surface Products over the Ocean and Implications for Uncertainties in Air-
953 Sea Boundary Forcing. *Journal of Climate*. 26. 153-170. 10.1175/JCLI-D-12-00090.1.

954 Large, W.G., Yeager, S.G. (2009). The global climatology of an interannually varying air–sea flux
955 data set. *Clim Dyn* 33, 341–364. 10.1007/s00382-008-0441-3